# POLITECNICO DI TORINO

Collegio di Ingegneria Chimica e dei Materiali

**Corso di Laurea Magistrale**
**in Ingegneria Chimica e dei Processi Sostenibili**

Tesi di Laurea Magistrale

# Polymer composites with cellulosic fillers: a study on gas transport properties

**Relatori**

Prof.ssa Roberta Maria Bongiovanni
Dott.ssa Alessandra Vitale
Dott.ssa Sara Dalle Vacche

**Candidato**

Luca Grillo

Marzo 2021

*Al nonno Bruno*

## ***Riassunto in italiano***

Lo scopo principale di questa tesi è quello di studiare il trasporto di gas all'interno di materiali compositi formati da una matrice polimerica rinforzata con filler cellulosici. In particolare, la parte sperimentale del lavoro ha avuto come obbiettivo l'analisi delle proprietà barriera verso l'ossigeno di un composito ottenuto da un lattice di origine naturale in cui sono state inserite microfibrille di cellulosa (MFC).

L'elaborato è stato suddiviso in diverse sezioni per migliorare la comprensione e la scorrevolezza degli argomenti trattati. Nella prima parte introduttiva viene descritta la cellulosa e i nanomateriali che possono essere ricavati da essa. Segue la descrizione del modello di permeazione con cui è stato trattato il trasporto di gas all'interno di materiali polimerici. Dopo aver descritto brevemente la permeabilità dei materiali nanocompositi, questa prima parte si conclude con una raccolta dei dati di letteratura relativi alla permeabilità dei principali materiali prodotti con la nanocellulosa. Nella seconda parte dell'elaborato vengono descritti i materiali e i metodi di caratterizzazione che sono stati applicati nello studio sperimentale. I risultati dell'indagine sono riportati e discussi nella terza sezione della tesi. Le conclusioni di questo studio sono riassunte nella quarta e ultima parte dell'elaborato.

Negli ultimi anni, la crescente consapevolezza dell'impatto ambientale causato dall'utilizzo della plastica di origine petrolchimica ha spinto la ricerca scientifica a sviluppare nuovi materiali alternativi da fonti rinnovabili. Il settore del packaging è responsabile di quasi il 40% della plastica prodotta in Europa, per cui è un reparto fondamentale su cui bisogna intervenire per ridurre l'inquinamento da plastica. Nel 2018, in Europa sono stati recuperati oltre 17 milioni di tonnellate di rifiuti plastici derivanti dall'imballaggio e di questi solo il 42% è stato riciclato. Avendo come target il raggiungimento di un tasso di riciclaggio dei rifiuti plastici del 55% entro il 2030, la Strategia europea per la plastica nell'economia circolare ha tra i suoi obbiettivi lo sviluppo di materiali innovativi in grado di competere con la plastica tradizionale. Il progetto comBIOsites, finanziato dalla comunità europea nell'ambito del programma MSCA – IF, si inserisce in questa strategia avendo come obbiettivo lo sviluppo di materiali compositi riciclabili che trovino impiego nel settore degli imballaggi. La tesi qui presentata ha svolto lo studio sperimentale delle proprietà barriera di un composito realizzato nell'ambito di questo progetto.

Nella produzione del composito studiato, come fase dispersa sono state impiegate delle microfibrille di cellulosa (MFC). La cellulosa è uno dei polimeri di origine naturale più abbondanti sulla terra e può essere ottenuta da diverse fonti rinnovabili. Dalle fibre di cellulosa possono essere ricavati dei nanomateriali tra i quali vi sono appunto le MFC. Questa tipologia di nanocellulosa si ottiene attraverso dei trattamenti meccanici che hanno lo scopo di disgregare la struttura della fibra di cellulosa.

Le MFC sono adatte sia per produrre film di semplice cellulosa, detti nanopaper, sia per essere usate come filler in nanocompositi. Per quanto riguarda i nanopaper di cellulosa, questi materiali si possono ottenere a partire da sospensioni acquose delle microfibrille. Quando l'acqua viene rimossa, si crea una rete tra le nanofibre di cellulosa grazie alla formazione di legami a idrogeno tra i gruppi ossidrili presenti nella struttura del cellobiosio, l'unità ripetitiva del polimero di cellulosa. Grazie a questi legami, i film di MFC godono di una bassa permeabilità nei confronti dell'ossigeno. Viceversa, i nanopaper risultano molto permeabili al vapor d'acqua. Infatti, la presenza dei gruppi ossidrili rende la cellulosa un

materiale altamente idrofilo, per cui condizioni di alta umidità relativa possono peggiorare le proprietà barriera dei film di MFC.

A causa dell'elevata sensibilità nei confronti dell'acqua, i nanopaper non hanno ancora trovato largo impiego come materiale per imballaggio. Un uso più promettente delle microfibrille di cellulosa risiede nel loro utilizzo sottoforma di filler all'interno di materiali nanocompositi. Un nanocomposito è un materiale polifasico in cui la fase dispersa ha almeno una dimensione nel range nanometrico (1-100 nm). Rispetto ai materiali compositi convenzionali, i nanocompositi mostrano migliori proprietà meccaniche, termiche e barriera anche a basse percentuali di rinforzo. Tuttavia, il carattere idrofilo della cellulosa può dare origine a delle problematiche anche nello sviluppo di materiali compositi con filler cellulosici. Infatti, poiché la maggior parte dei materiali polimerici è idrofoba, l'ottenimento di una buona dispersione delle microfibrille di cellulosa all'interno di una matrice polimerica non è sempre garantito. La ricerca scientifica ha sviluppato diverse strategie con l'obbiettivo di aumentare la compatibilità tra nanocellulosa e polimeri idrofobi. Tra le tecniche più utilizzate vi sono dei trattamenti superficiali che hanno lo scopo di rendere le fibre di cellulosa più idrofobe, oppure si possono impiegare degli agenti di accoppiamento.

Nel caso specifico del materiale composito che è stato analizzato sperimentalmente in questo studio, non si è dovuto ricorrere a nessuna modificazione per migliorare la compatibilità tra le microfibrille e la matrice polimerica. Infatti, quest'ultima è costituita da un lattice ottenuto tramite un processo di polimerizzazione in emulsione acquosa per cui l'inserimento delle MFC è avvenuto semplicemente miscelando la sospensione delle microfibrille all'interno del lattice.

Uno degli obbiettivi principali che ha spinto lo sviluppo di questo lattice naturale rinforzato con MFC è un suo potenziale impiego come materiale per imballaggio. Tra le varie funzioni che deve svolgere il packaging, la funzione di barriera nei confronti di possibili contaminanti esterni è una delle più importanti. Soprattutto in ambito alimentare, l'imballaggio deve avere proprietà tali da impedire il trasporto di gas come il vapor d'acqua o l'ossigeno, che potrebbero portare al deterioramento dell'alimento imballato.

Il trasporto di gas all'interno di materiali polimerici può essere descritto tramite il modello della permeazione. Questo fenomeno avviene perché le molecole di gas/vapore permeano il volume libero inter/intramolecolare del polimero, ovvero quella frazione del volume specifico di un polimero che non è occupato dalle molecole. Il processo di permeazione può essere suddiviso in tre passaggi:

1. Adsorbimento: il gas si scioglie all'interfaccia del polimero seguendo la legge di Henry.
2. Diffusione: la molecola di permeante diffonde all'interno del materiale secondo la prima legge di Fick.
3. Desorbimento: raggiunta l'altra interfaccia del polimero, il permeante si desorbe sempre secondo la legge di Henry.

L'intero meccanismo di permeazione è rappresentato schematicamente in Figura 1**.** Nello schema viene considerato un sistema monodimensionale in cui la permeazione avviene solo lungo lo spessore $L$ di un film polimerico di area $A$. Il film è esposto a un generico permeante che ha una pressione parziale pari a $p_1$ da un lato e una pressione parziale $p_2$ dall'altro lato del film, con $p_1 > p_2$. Il gas si discioglie all'interfaccia del polimero e, a causa del gradiente di concentrazione, diffonde all'interno del film.

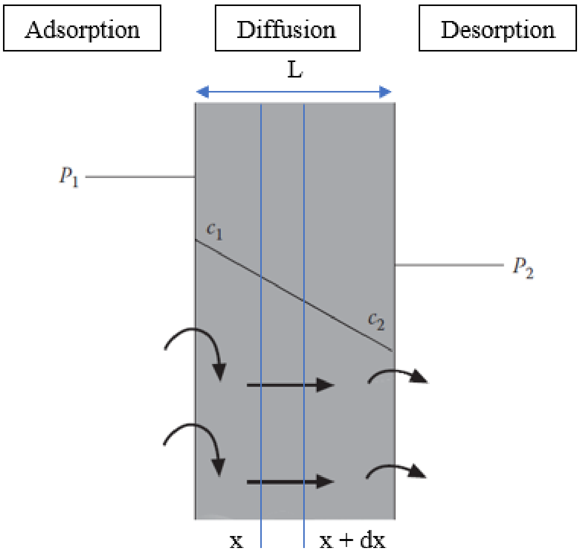

Figura 1: Schema del processo di permeazione di un gas/vapore all'interno di un film polimerico

Il *coefficiente di diffusione D* e il *coefficiente di solubilità S* del permeante all'interno del polimero entrano nella definizione del cosiddetto *coefficiente di permeabilità $K_P$* del polimero verso uno specifico gas/vapore. $K_P$ è infatti dato dal prodotto dei due coefficienti che regolano i meccanismi di diffusone e di adsorbimento/desorbimento, come mostrato nell'Equazione (1).

$$K_P = D \cdot S \tag{1}$$

Una definizione alternativa del coefficiente di permeabilità è data nell'Equazione (2).

$$K_P = \frac{q \cdot L}{A \cdot t \Delta p} \tag{2}$$

Dove *q* è il quantitativo di gas che permea un film di spessore *L* e superficie *A* nell'unità di tempo *t* a seguito della presenza di un gradiente di pressione parziale del permeante *Δp* tra i due lati del film polimerico. Oltre al coefficiente di permeabilità, un altro parametro molto diffuso usato per descrivere le proprietà barriera di un materiale è la *Gas Transmission Rate (GTR),* la cui definizione è riporta in Equazione (3).

$$GTR = \frac{q}{A \cdot t} \tag{3}$$

Esistono vari metodi sperimentali per valutare le proprietà barriera di un materiale. Tra le apparecchiature più adottate, quella principale è costituita da una cella che viene divisa in due camere separate dal film di cui si vuole valutare la permeabilità. Nel metodo differenziale di conduzione del test, una corrente di gas test a composizione nota viene mandata nella camera superiore delimitata dal film. In quella inferiore, invece, si manda un gas di trasporto che non contiene il permeante. In questo modo, si genera un gradiente nella pressione parziale del gas permeante che provoca il fenomeno di permeazione. Un detector misura la corrente di permeante che esce dalla camera sottostante e che deriva dal trasporto di gas avvenuto attraverso il film esaminato. Una rappresentazione schematica della cella sperimentale adottata nel metodo differenziale si può trovare nella Figura 2.

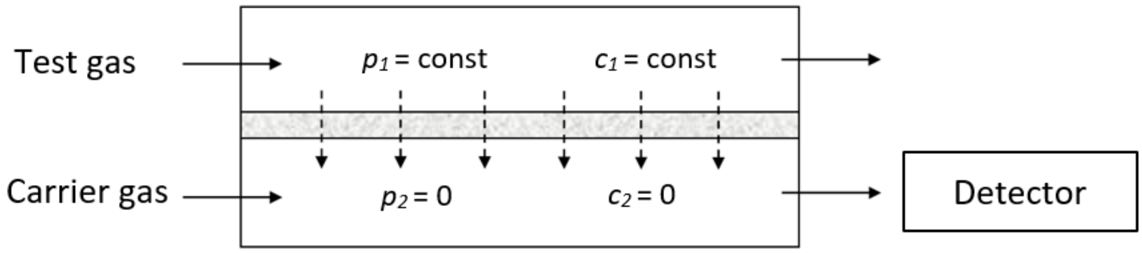

Figura 2: Schema di una generica cella sperimentale usata per un test differenziale di permeabilità

Dall'analisi dei dati sperimentali raccolti durante la prova differenziale, si possono ricavare sia il coefficiente di permeabilità $K_P$ sia il coefficiente di diffusione $D$.

Per migliorare le proprietà barriera di un materiale polimerico, la strategia più adottata consiste nell'incorporare una seconda fase all'interno della matrice polimerica. Nel caso di materiali compositi, l'inserimento di filler inerti provoca un aumento della tortuosità del percorso diffusivo di un permeante all'interno del materiale rinforzato. La presenza dei filler, infatti, costringe le molecole di permeante a deviare la propria traiettoria durante il processo di diffusione e questo effetto provoca una diminuzione della permeabilità del materiale polimerico. Affinché si ottenga questo miglioramento nelle proprietà barriera, i filler devono essere dispersi nella fase continua senza che si creino separazioni di fase né agglomerati. Nel caso delle microfibrille di cellulosa, una loro dispersione in polimeri idrofobi potrebbe essere compromessa dalla natura idrofila propria delle MFC. A seconda quindi del materiale che si sceglie di rinforzare, possono essere necessari dei trattamenti per migliorare la compatibilità tra fase dispersa e fase continua.

Siccome la cellulosa può essere estratta da numerose fonti rinnovabili, sono stati svolti numerosi studi sulle proprietà barriera dei principali materiali che si possono ottenere a partire dalla nanocellulosa, avendo come obbiettivo un loro impiego nel settore del packaging. Considerando dapprima i nanopaper di cellulosa, questi hanno mostrato alte proprietà barriera nei confronti dell'ossigeno, mentre nei confronti del vapor d'acqua non riescono a competere con i polimeri di origine petrolchimica, che sono oggigiorno i più utilizzati negli imballaggi. Per quanto riguarda invece i materiali nanocompositi con filler cellulosici, dai dati raccolti in letteratura è risultato evidente che all'aumentare del contenuto di cellulosa si ha un miglioramento delle proprietà barriera, sia nei confronti dell'ossigeno sia nei confronti del vapor d'acqua.

Dopo aver valutato la potenzialità dei filler cellulosici nel migliorare le proprietà barriera di materiali nanocompositi, è stata condotta un'indagine sperimentale sulla permeabilità all'ossigeno di un materiale composito rinforzato con microfibrille di cellulosa. Sono state impiegate delle MFC commerciali Exilva 01-V (abbreviate in seguito con EV), fornite con una concentrazione del 10% in peso. Per quanto riguarda la matrice polimerica, sono state usate due tipologie di polimeri. Nella prima parte dello studio è stato utilizzato un lattice di origine naturale, prodotto a partire dal metacrilato di un derivato dell'eugenolo, l'etossi diidroeugenil metacrilato (EDMA). L'EDMA è stato fornito con un contenuto solido totale (TSC) del 15%. Nella seconda parte dello studio si è usato un copolimero di EDMA con l’1% di cumarina, sempre sottoforma di lattice, abbreviato in seguito con EDMA-C1. L’EDMA-C1 è stato fornito con un 16,5% di TSC.

Il primo step per la preparazione del nanocomposito consiste nella diluizione della pasta di MFC in acqua distillata per ottenere una sospensione acquosa che possa essere miscelata insieme al lattice. Per rendere la sospensione delle microfibrille più omogenea si è impiegato un omogenizzatore T 10 ULTRA-TURRAX®. Ottenuta la concentrazione desiderata di MFC in acqua, la sospensione viene aggiunta al lattice. Per disperdere in maniera omogenea la sospensione di MFC all’interno del lattice è stato utilizzato un agitatore magnetico. Dopo la fase di agitazione, la miscela viene sottoposta al vuoto per rimuovere eventuali bolle d’aria che potrebbero provocare poi dei difetti nel film di composito. Dopo il degassaggio, la soluzione viene versata in un disco di Petri e lasciata asciugare sotto cappa per almeno una notte. Nel seguito della trattazione, i compositi verranno indicati tramite una notazione che riporta: la matrice polimerica (EDMA o EDMA-C1), il contenuto di MFC (EV30 o EV5) e la concentrazione di microfibrille nella sospensione usata per la preparazione del composito.

Dopo l’evaporazione dell’acqua, per rimuovere eventuali increspature che potrebbero compromettere la caratterizzazione dei film, alcuni campioni dei compositi sono stati sottoposti a una leggera pressatura a caldo. Nello specifico, sui film è stata applicata una pressione di 76 [mbar] a 85 [°C] per 1,5 ore. I compositi ottenuti con EDMA-C1 sono stati poi sottoposti a un irraggiamento con raggi UV per stimolare una reazione di reticolazione all’interno del materiale, data nello specifico dal processo reversibile di foto-dimerizzazione della cumarina. I film in questione sono stati soggetti a 20 [mW/cm$^2$] for 20 minuti.

Per valutare il grado di dispersione delle MFC all’interno del lattice, i film ottenuti sono stati osservati al microscopio ottico. Prima di procedere con ulteriori caratterizzazioni dei compositi, è stata fatta una selezione dei vari film ottenuti. Nello specifico, si è scelto di effettuare le misure di energia superficiale e di permeabilità sui compositi ottenuti usando una sospensione delle MFC al 0,75% in peso perché sono quelli che apparivano più omogenei. È stato caratterizzato anche il film di EDMA-EV5-1, l’unico film ottenuto inserendo il 5% di MFC all’interno del lattice di EDMA. Riassumendo, i film selezionati per la valutazione dell’energia superficiale e della permeabilità all’ossigeno sono: EDMA-EV5-1, EDMA-EV30-0,75, EDMA-C1-EV5-0,75 ed EDMA-C1-EV30-0,75.

La superficie dei film selezionati è stata caratterizzata attraverso la valutazione dell’energia superficiale. Quest’ultima è stata calcolata attraverso il metodo di Owens-Wendt, basato sulla misura degli angoli di contatto del film con due liquidi diversi, in questo caso acqua ed esadecano. Gli angoli di contatto sono stati misurati con FTA1000 C Drop Shape Instrument a temperatura ambiente. Le immagini delle gocce di liquido sono state poi analizzate con il software FTA 32.

Per quanto riguarda la valutazione della permeabilità all’ossigeno, i test sono stati condotti con un permeometro Multi Perm: Oxygen & Water Vapor Permeability Analyser (MULTI 01/02/O2/H2O, ExtraSolution S.r.l.). Questo strumento esegue un test di permeabilità di tipo differenziale usando come gas test una corrente di ossigeno, mentre come gas di trasporto utilizza una corrente di azoto. Il risultato del test viene fornito nella forma di Oxygen Transmission Rate (OTR) espressa in [cc/(m$^2$ d)]. I film analizzati sono stati inseriti in un riduttore di superficie di 2,01 [cm$^2$] e il loro spessore è stato calcolato con un micrometro. I test sono stati condotti a una temperatura T = 23 [°C] e un’umidità relativa RH = 0%. Per effettuare una stima del coefficiente di diffusione del gas all’interno dei compositi, i dati sperimentali sono stati analizzati attraverso due metodi: il metodo del time-lag, basato sulla soluzione della cosiddetta seconda legge di Fick e adattato al test differenziale, e un metodo grafico basato sull'identificazione del punto di half-time, ovvero l'istante di tempo in cui si raggiunge la metà del valore asintotico di OTR.

Tutti i film dei compositi ottenuti appaiono abbastanza trasparenti. A titolo di esempio, la Figura 3 mostra il film di EDMA-C1-EV5-0,75.

Figura 3: Film di EDMA-C1-EV5-0,75

L'aspetto opaco che si può osservare nella foto a destra della Figura 3 è dovuto probabilmente alla diffusione ottica (light scattering). Questo fenomeno visivo può essere provocato dall'eterogeneità della superficie dei compositi e dalla rugosità superficiale del film.

Il film di EDMA-C1-EV5-0,75 ha presentato dei punti in cui è stata osservata una scarsa inclusione di MFC, confermata dalle immagini prese al microscopio ottico come quella riportata in Figura 4a. Queste zone con assenza di MFC possono essere dovute alla blanda miscelazione che è stata usata per disperdere le microfibrille nel lattice. Infatti, per evitare un'eccessiva inclusione d'aria che avrebbe creato delle porosità nei film di composito, nella preparazione dei compositi sono state usate basse velocità di agitazione.

Nonostante la presenza di alcune zone prive di MFC, nella maggior parte del composito le microfibrille sono risultate disperse molto bene all'interno della matrice polimerica. La Figura 4b mostra inoltre che si è formata una sorta di rete tra le nanofibre di cellulosa. Questa struttura disordinata generata dalle microfibrille aumenta la tortuosità interna al film di composito, che era appunto l'obbiettivo dell'inserimento delle MFC all'interno del lattice. Anche altri film di composito hanno mostrato la formazione di questa rete di microfibrille che dovrebbe migliorare le proprietà barriera del materiale.

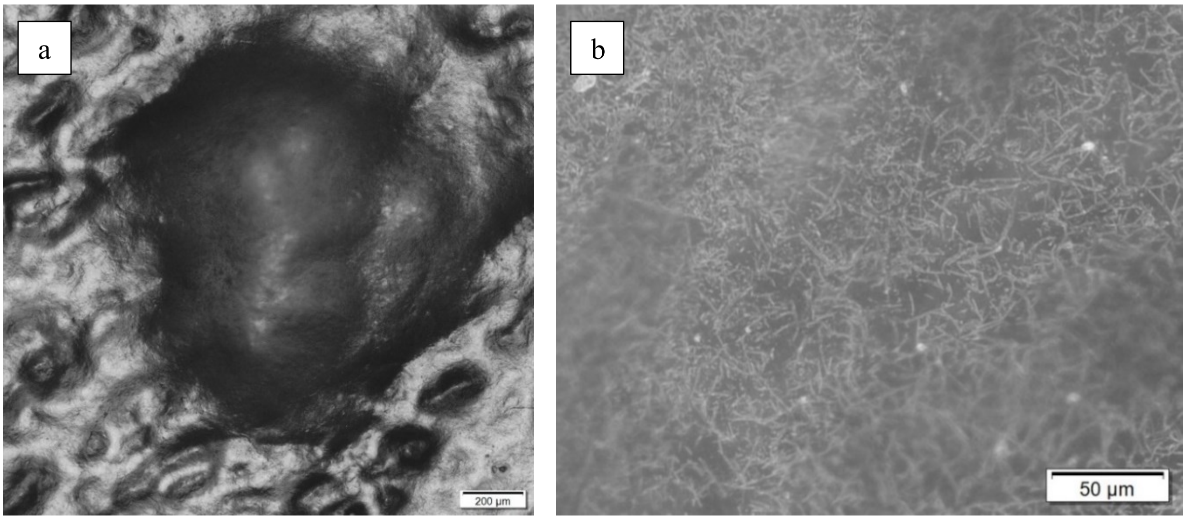

Figura 4: Osservazioni al microscopio ottico di EDMA-C1-EV5-0,75

Dopo la procedura di pressatura a caldo, i film sono risultati più appiattiti e quindi più idonei per le successive caratterizzazioni legate alla misura degli angoli di contatto e al test di permeabilità. Le osservazioni al microscopio sono state ripetute per valutare eventuali cambiamenti nella morfologia dei compositi. Mentre i compositi contenenti un 5% di MFC hanno mantenuto al loro interno quella struttura a rete osservata in Figura 4b, le immagini prese al microscopio dei compositi con 30% di MFC hanno mostrato la presenza di alcuni agglomerati di microfibrille. Nonostante ciò, dopo la pressatura a caldo i compositi hanno mantenuto una buona tortuosità interna data dalle microfibrille.

Per quanto riguarda il processo di reticolazione tramite irraggiamento UV, questo ha avuto effetti visibili solo su uno dei due campioni di composito dell'EDMA-C1 sottoposti a questa procedura. Mentre il campione contenente il 5% di MFC ha assunto una colorazione più gialla dopo l'esposizione ai raggi UV, quello con il 30% di microfibrille non ha mostrato nessun cambiamento evidente che potesse indicare l'avvenuta reticolazione. Probabilmente, il maggiore contenuto di cellulosa ha impedito una variazione visibile nel colore del film.

Oltre ai compositi di EDMA e di EDMA-C1, le misure degli angoli di contatto con acqua ed esadecano sono state effettuate anche su dei film di MFC e di EDMA puri per avere un termine di paragone. Per quanto riguarda il film ottenuto dal lattice di EDMA, questo ha mostrato un angolo di contatto con l'acqua di soli 31 [°]. Poiché il lattice conteneva un 4% di sodio dodecilsolfato (SDS) rispetto al peso del polimero di EDMA, si è ipotizzato che la presenza del tensioattivo in superficie avesse abbassato il valore dell'angolo di contatto. Per verificare questa ipotesi, il film di EDMA è stato immerso in acqua distillata e la misura dell'angolo di contatto è stata ripetuta dopo l'asciugatura del film. Dopo il bagno, il valore dell'angolo di contatto è aumentato sino a un valore di 65 [°], il che potrebbe confermare che la presenza di tracce di SDS sulla superficie del film abbia causato un angolo di contatto inferiore nella misura iniziale.

Per quanto riguarda i compositi del lattice, i valori calcolati relativi agli angoli di contatto sono risultati intermedi rispetto a quelli registrati con i film di EDMA e di MFC puri. I compositi contenenti una maggiore percentuale di MFC hanno riscontrato degli angoli di contatto con l'acqua molto più elevati rispetto a quelli registrati con in compositi con basso contenuto di microfibrille, con differenze anche di 20 [°]. Anche questa differenza potrebbe essere dovuta alla presenza di SDS nel lattice. È possibile che nei compositi con solo il 5% di MFC, delle tracce di tensioattivo siano rimaste presenti in superficie, provocando dei valori più bassi degli angoli di contatto con l'acqua. Invece, nei compositi con il 30% di MFC, le microfibrille potrebbero aver attratto la parte idrofila dell'SDS, impedendone la riorentazione verso la goccia d'acqua e quindi riducendo l'effetto bagnate del tensioattivo. Un altro fattore che potrebbe spiegare la differenza riscontrata negli angoli di contatto tra compositi con diverse percentuali di MFC è la rugosità superficiale. Un maggiore contenuto di microfibrille potrebbe aver provocato una maggiore rugosità e questa potrebbe spiegare i diversi valori degli angoli di contatto nei compositi con contenuti diversi di MFC. Per poter effettuare un'analisi più accurata sui diversi fattori che determinano l'energia superficiale di un solido, sarebbero necessarie caratterizzazioni più approfondite della superficie dei film esaminati, in modo da avere dati più precisi sulla composizione e sulla rugosità superficiale.

Nello studio delle proprietà barriera dei compositi selezionati, è stato imposto un tempo minimo di condizionamento di 20 ore per ogni misura in modo da avere dei risultati affidabili. Il condizionamento è la fase che precede la misura effettiva di OTR in cui in entrambe le camere della cella sperimentale viene mandata una corrente di azoto per eliminare l'ossigeno che è stato introdotto quando è stato caricato il film da esaminare. Grazie a questo accorgimento, le curve sperimentali non hanno dato segni di incongruenza rispetto all'andamento teorico e hanno raggiunto un valore stabile di OTR in meno di due ore, come dimostra il grafico riportato in Figura 5 che mostra la misura effettuata sul composito EDMA-C1-EV5-0,75. Considerando i tempi elevati richiesti per una singola misurazione, nella sola settimana in cui il permeometro è stato reso disponibile sono state svolte solamente poche prove di permeabilità.

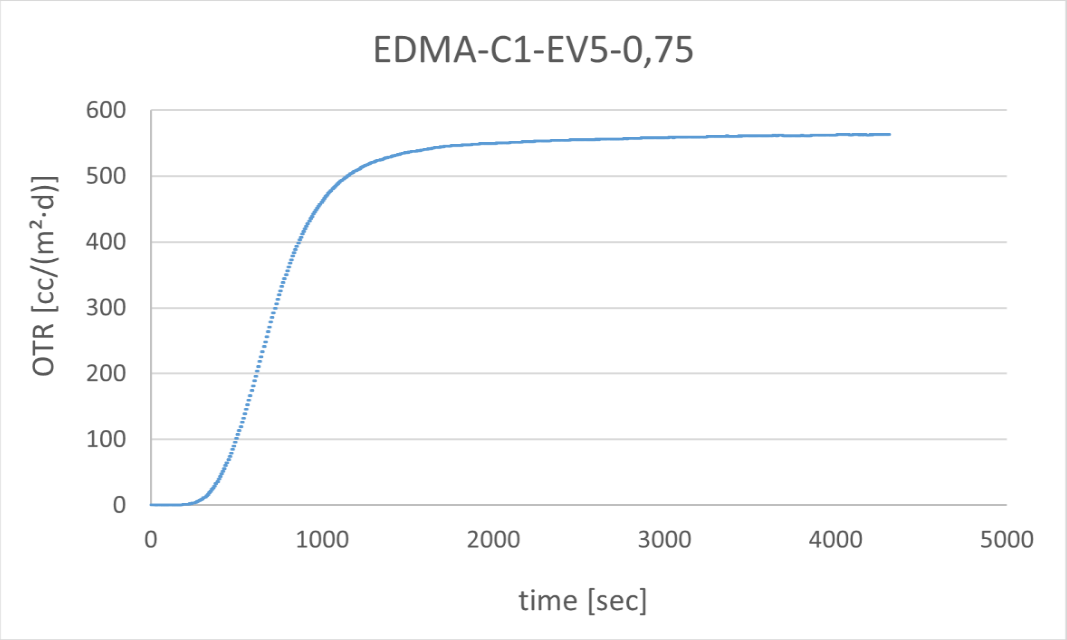

Figura 5: Curva sperimentale dell'OTR del film di EDMA-C1-EV5-0,75

Non essendo stato possibile produrre un film di lattice EDMA puro con dimensioni idonee per effettuare i test di permeabilità, per valutare l'effetto del contenuto di MFC sono stati indagati compositi con due percentuali diverse di microfibrille. Siccome i diversi film avevano spessori differenti, per avere un confronto più oggettivo sui risultati dei test, i valori sperimentali dell'Oxygen Transmission Rate sono stati normalizzati a uno spessore standard di 25 [μm] e verranno in seguito indicati come $OTR_{25}$.

L'aumento del contenuto di MFC dal 5% al 30% ha provocato un abbassamento del 71% nell'$OTR_{25}$ dei compositi di EDMA e una riduzione del 68% in quelli di EDMA-C1. Questo abbassamento della permeabilità conferma l'ipotesi che l'aggiunta di microfibrille provoca un miglioramento nelle proprietà barriera di un materiale polimerico.

Poiché questo miglioramento è stato attribuito a una maggiore tortuosità data dall'inserimento dei filler all'interno delle matrici di lattice, l'effetto dei due diversi contenuti di MFC è stato valutato anche sul coefficiente di diffusione $D$. Facendo un confronto sui valori di $D$ ottenuti con il metodo del time-lag, ritenuto più accurato, i compositi di EDMA hanno mostrato un abbassamento dell'84% nella diffusività a seguito di un incremento del contenuto di MFC. Nei compositi di EDMA-C1, passando dal 5% al 30% di microfibrille, il coefficiente di diffusione è diminuito dell'80%. Questi risultati confermano l'ipotesi secondo cui la presenza dei filler cellulosici aumenta la tortuosità del percorso diffusivo del gas permeante all'interno di una matrice polimerica. È possibile che un contenuto ancora maggiore di MFC possa provocare un miglioramento ulteriore nelle proprietà barriera del composito.

A parità di contenuto di microfibrille, i compositi ottenuti con il copolimero EDMA-C1 hanno mostrato dei valori di $OTR_{25}$ che sono la metà di quelli misurati per i compositi di EDMA. Poiché la differenza tra le due matrici polimeriche non ha dato segni così significativi sui coefficienti di diffusione, la minore permeabilità riscontrata con i compositi di EDMA-C1 è stata attribuita a un effetto della cumarina sulla solubilità dell'ossigeno nel lattice. Nella struttura del copolimero di EDMA-cumarina è presente un maggior numero di gruppi polari che potrebbero causare una riduzione della solubilità di un gas apolare come l'ossigeno. Inoltre, le interazioni deboli che si possono instaurare tra le catene del copolimero potrebbero aver ridotto il volume libero della matrice polimerica e aver abbassato la permeabilità dei compositi di EDMA-C1.

Un'altra strategia che è stata sperimentata per ridurre la permeabilità dei compositi di EDMA-C1 è la reticolazione. Con la formazione di nuovi legami trasversali tra le catene, il volume libero del polimero dovrebbe diminuire e così anche la sua permeabilità. Per valutare l'effetto della reticolazione sulle proprietà barriera del materiale sviluppato, i compositi di EDMA-C1 sono stati sottoposti ad irraggiamento UV con lo scopo di stimolare la foto-dimerizzazione della cumarina. Questa procedura è stata applicata direttamente sui campioni di EDMA-C1-EV5-0,75 e EDMA-C1-EV30-0,75 che erano stati usati in test di permeabilità precedenti. Dopo la reticolazione, l'OTR dei due compositi non ha subito un cambiamento così marcato. Con EDMA-C1-EV5-0,75, l'OTR si è ridotta da 561 [cc/$m^2$ d] a 533 [cc/$m^2$ d], mentre l'OTR di EDMA-C1-EV30-0,75 è passata da 399 [cc/$m^2$ d] a 300 [cc/$m^2$ d]. Questo scarso effetto della reticolazione potrebbe essere dovuto al fatto che il copolimero di EDMA-C1 contiene solamente l'1% di cumarina e quindi la reticolazione data dalla sua foto-dimerizzazione non è stata così diffusa nella matrice del composito. Probabilmente, usando un copolimero di EDMA con un maggiore contenuto di cumarina, la reticolazione potrebbe dare un miglioramento più marcato sulle proprietà barriera del materiale.

Per valutare se il materiale composito sviluppato possa competere con i polimeri di origine petrolchimica che sono maggiormente usati negli imballati, i dati di permeabilità all'ossigeno registrati dai composti esaminati sono stati confrontati con quelli di alcune plastiche tradizionali. Il confronto è avvenuto con dati di letteratura che fanno riferimento a valori di $OTR_{25}$ valutati nelle stesse condizioni studiate in questo lavoro sperimentale: temperatura T = 23 [°C] e umidità relativa RH = 0%. Tra i compositi analizzati in questo studio, solo EDMA-C1-EV30-0,75 ha mostrato dei valori competitivi dell'$OTR_{25}$. Nello specifico, prima della reticolazione il composito ha registrato un valore di $OTR_{25} = 827$ [cc/$m^2$ d]. Questo valore è molto inferiore rispetto a quello di polimeri come il polietilene o il polipropilene, mentre risulta più elevato se paragonato con l'$OTR_{25}$ del PET o del nylon 6,6. In definitiva, si può dire che il composito ottenuto con l'EDMA-C1 e un 30% di MFC ha medie proprietà barriera nei confronti dell'ossigeno. In ogni caso, per valutare l'effettiva validità di questo materiale in una possibile applicazione per il packaging, si dovrebbero analizzare le sue proprietà barriera anche nei confronti di altri gas come l'anidride carbonica o il vapor d'acqua, anche in funzione di diverse condizioni esterne di temperatura e umidità relativa.

Un fattore molto importante che contraddistingue il composito sviluppato in questo studio e il resto dei polimeri tradizionali usati per gli imballaggi è la sostenibilità ambientale che caratterizza entrambi i componenti del composito. Per quanto riguarda la matrice polimerica, questa consiste di un lattice di origine naturale ricavato dal metacrilato di un derivato dell'eugenolo. L'eugenolo è un fenolo naturale che può essere estratto da numerose risorse vegetali rinnovabili. Anche il processo di produzione del lattice è sostenibile perché sfrutta un processo di polimerizzazione in emulsione acquosa. Questa tecnica di polimerizzazione, infatti, non richiede l'utilizzo di solventi dannosi per l'ambiente ed è quindi considerato come un processo a basso impatto ambientale. Per quanto riguarda i filler impiegati come rinforzo, le microfibrille di cellulosa sono biodegradabili e possono essere prodotte a partire da un elevato numero di risorse rinnovabili. L'impiego nel settore del packaging di materiali biodegradabili e prodotti a partire da risorse rinnovabili potrebbe ridurre sia la dipendenza da polimeri di origine petrolchimica, sia migliorare lo smaltimento dei rifiuti plastici, apportando un doppio beneficio all'ambiente.

Con questa tesi è stato possibile analizzare il ruolo dei filler cellulosici nel trasporto di gas all'interno di compositi polimerici.

Dai dati raccolti in letteratura, sono emerse le potenzialità della nanocellulosa come materiale di rinforzo per migliorare le proprietà barriera di diverse matrici polimeriche. L'inserimento di nanofiller, infatti, aumenta la tortuosità del percorso diffusivo di un gas e riduce quindi la permeabilità del materiale in cui sono stati inseriti.

Sperimentalmente, si è osservato che all'aumentare del contenuto di microfibrille di cellulosa, la permeabilità all'ossigeno del materiale composito indagato è diminuita del 70% in termini di Oxygen Transmission Rate. Questo miglioramento delle proprietà barriera è stato confermato anche da un abbassamento del coefficiente di diffusione dell'ossigeno all'interno del composito. Aumentando il contenuto di microfibrille dal 5% al 30%, la diffusività nei compositi indagati è diminuita dell'80%. Questi due aspetti dimostrano che l'effetto principale dato dall'inserimento delle MFC risiede nell'aumentare la tortuosità del percorso diffusivo di un permeante, che a sua volta provoca un abbassamento della permeabilità. Probabilmente, l'inserimento di una maggiore quantità di microfibrille potrebbe dare un ulteriore miglioramento delle proprietà barriera dei materiali compositi.

Un’altra strategia che è stata analizzata per ridurre la permeabilità all’ossigeno dei film sviluppati è stata la reticolazione dei compositi ottenuti con il lattice di EDMA-C1. La formazione di legami trasversali tra le catene del polimero, infatti, dovrebbe ridurre il volume libero disponibile alla permeazione di gas. Tuttavia, questa procedura non ha dato dei miglioramenti così evidenti nelle proprietà barriera dei compositi. Nel migliore dei due casi analizzati, l’OTR è diminuita solo del 25% dopo reticolazione. Probabilmente, lo scarso effetto registrato è dovuto al fatto che il copolimero EDMA-C1 usato come matrice contiene solo l’1% di cumarina. Siccome è la reazione di foto-dimerizzazione della cumarina a generare legami trasversali nel copolimero, un contenuto così basso di questo composto aromatico potrebbe non aver garantito una reticolazione diffusa all’interno della matrice di lattice. Verosimilmente, se si usasse come matrice un copolimero con una maggiore percentuale di cumarina, l’effetto della reticolazione potrebbe essere più pronunciato.

Infine, nel confronto con le plastiche tradizionali impiegate nel packaging, solo il composito EDMA-C1-EV30-0,75 ha mostrato di avere proprietà barriera contro l’ossigeno competitive. Tuttavia, per valutare un suo effettivo impiego come materiale per imballaggi, sono necessarie ulteriori indagini.

Con questa prospettiva futura, si potrebbero condurre dei test per valutare le proprietà barriera del materiale composito sviluppato nei confronti di altri gas come l’anidride carbonica o il vapor d’acqua. Inoltre, sarebbe utile indagare l’effetto delle condizioni esterne di temperatura e umidità relativa sulla permeabilità del materiale. Infine, per valutare in maniera più approfondita l’effetto delle microfibrille di cellulosa e della reticolazione, si potrebbero analizzare compositi con composizioni diverse sia per quanto riguarda la percentuale di filler cellulosici sia per quanto riguarda la percentuale di cumarina.

# Table of contents

# 1. Introduction

## *1.1 Preface*

In 2018, almost 360 million tons of plastics were produced in the world, only in Europe plastics production reached 61,8 million tons. The packaging industry is responsible for almost 40% of this production [1], therefore it is a key sector where action must be taken to reduce the environmental impact caused by plastic pollution and the use of fossil resources.

Indeed, the packaging industry nowadays relies on the use of petroleum-based materials because they have features particularly suitable for packaging application: transparency, ease of processing, thermal performance, high barrier properties and low cost [2]. Despite these useful characteristics, plastics have serious environmental drawbacks: non-biodegradability and the associated waste management issues. In 2018, 17,8 million tons of plastic post-consumer packaging waste were collected in Europe to be treated, but only 42% of these were recycled. The remaining 39,5% was used for energy recovery while 18,5% was sent to landfill [1] and this percentage is still too high.

In the European Strategy for Plastics in a Circular Economy [3] the European Commission has made several commitments including raising recycling rates of plastic packaging waste, having the following targets: a rate of 50 wt% within 2025 and 55 wt% within 2030 [4]. Another goal that has been set is the development of innovative materials produced from alternative raw materials that could compete with the traditional petrochemical sources for the plastic production.

Replacing traditional plastics with new biodegradable materials from renewable resources has many benefits. Firstly, using biodegradable polymers improves waste disposal, cutting the amount of plastic waste sent to incinerators and landfills. Moreover, the use of raw materials such as by-products from the agri-food industry may lead to a new circular economy for the plastic production, thus reducing the dependence on petroleum-based polymers [5].

ComBIOsites project, in the frame of the MSCA programme of the EU[1], well fits into this context since it aims at developing recyclable composite materials for packaging. The main raw material that has been studied for this objective is cellulose, more specifically Microfibrillated Cellulose (MFC) has been used to produce film with good barrier properties against gases. However, due to the high hydrophilicity of cellulose, the water vapor permeability of these films prevents them from being used at high relative humidity. For this reason, MFC has been used as filler combined with other polymers in the form of nanocomposites.

As part of the comBIOsites project, the main aim of this thesis is the study of barrier properties of the developed nanocomposite material. More specifically, the experimental part of this work aims at estimating the oxygen transmission rate (OTR) of a biobased latex reinforced with MFC.

The work has been divided into different sections in order to guarantee a better comprehension of the treated topics. In the first part, cellulosic nanomaterials are introduced and the gas transport through polymeric film is described in terms of permeability.

---

[1] The project ComBIOsites has received funding from the European Union’s Horizon 2020 research and innovation programme under the Marie Skłodowska-Curie grant agreement No789454 (http://www.h2020-combiosites.eu/)

Afterwards, the experimental section presents the materials and the methods adopted for the preparation and the characterization of the nanocomposite. Then, the results are reported and discussed in the third section while the fourth and last section collects the conclusions of the work.

## *1.2 Cellulose and cellulosic nanomaterials*

### 1.2.1 Cellulose and nanocellulose

Cellulose is one of the most abundant bio-based polymers on earth and it is widely distributed in several sources. In addition to wood, which is the main industrial source of cellulose, cellulosic fibers can be extracted from other higher plants such as cotton, sisal, flax, etc. Less important sources are also some marine animals, algae, fungi and bacteria [6].

Regardless of its origin, chemically cellulose is a linear homopolysaccharide of β-1,4-D-glucose and its repeating unit consists of a dimer called cellobiose. In nature, cellulose is characterized by a hierarchical structure organized in fibers. As reported in Lavoine et. al. [7], about 36 individual cellulose molecules make up the so-called elementary fibrils or microfibrils, which in turn assemble into a larger structure known as microfibrillated cellulose (MFC). The latter are brought together to form the macroscopic cellulosic fiber, as shown in **Figure 1.1**.

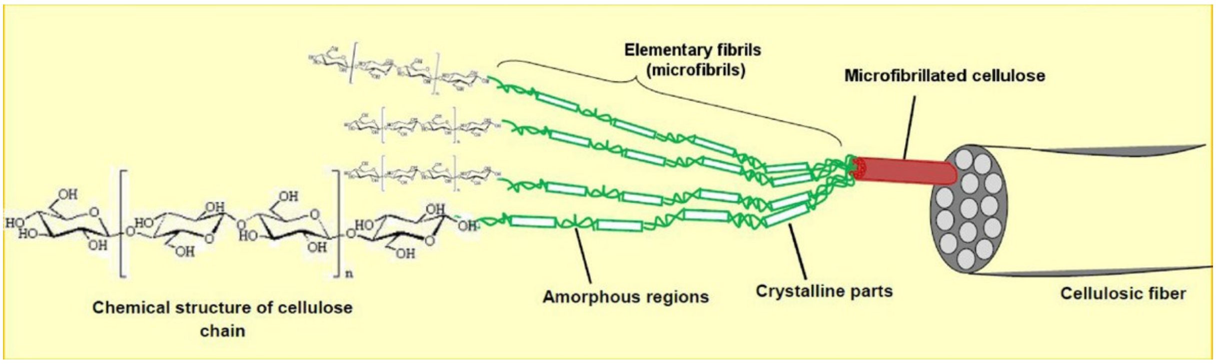

**Figure 1.1:** Hierarchical structure of cellulose fiber. With permission from *[7]*

**Figure 1.1** shows also that single microfibrils have a semicrystalline structure alternated between amorphous and crystalline domains. The latter are ordered regions where cellulose chains are stabilized by a robust network of hydrogen bonds originated among the hydroxyl groups within the monomer [8]. This kind of organization explains why there are two main types of nanocellulose: cellulose nanocrystals and microfibrillated cellulose.

Cellulose nanocrystals (CNC), also called cellulose whiskers, are obtained through an acid hydrolysis that preferentially attacks the amorphous regions of native cellulose, leading to the formation of crystals with high purity. On the other hand, microfibrillated cellulose (MFC), also referred to as nanofibrillated cellulose (NFC), shows both amorphous and crystalline domains and is produced with mechanical treatment. Actually, there is a third type of nanocellulose: bacterial cellulose (BC). Unlike CNC and MFC, that are obtained in a top-down process, BC is produced by some bacteria (e.g., Glunacetobacter xylinus) with a bottom-up method [7].

Among these three types of nanocellulose, MFC is particularly suitable both to be used as an independent material and as filler for nanocomposites and there are many studies in literature concerning its application in the packaging field [6] [9].

Microfibrillated cellulose can be manufactured from different cellulosic sources and wood is certainly the most important one. Although bleached kraft pulp and bleached sulfite pulp are the most used starting materials for MFC production, the competition from different sectors that use wood (e.g., building, paper industry, combustion, etc.) has aroused interest in other sources such as agricultural crops and their by-products. The use of non-wood sources such as sugar beet pulp, hemp, sisal and others has also some advantages. Firstly, cellulose microfibrils from agricultural fibers are easier to extract and thus the fibrillation should be less energy demanding [7]. Moreover, by-products from agri-food industry are renewable and low cost and their use as sources of nanocellulose fits in perfectly with the promotion of a sustainable and circular economy.

Regardless of the source, MFC is obtained from a pulp suspension that is treated with a mechanical process. The main mechanical treatment used for MFC production consists of a refining process followed by a high-pressure homogenization; the latter step can be performed either with a homogenizer [10] or with a microfluidizer [11]. In addition to this method, other two examples of mechanical treatment used for the fibrillation process are cryocrushing [12] and grinding [13]. A feature that all these methods have in common is their high energy consumption. This negative aspect is due to the fact that often several cycles of treatment are needed to obtain the desired degree of fibrillation and so the energy demand increases [7].

In order to lessen this drawback, the mechanical process is usually combined with a pre-treatment applied to cellulose fibers with the purpose to reduce the energy required for fibrillation. The most commonly used pre-treatments are the enzymatic hydrolysis with endoglucanase [14], the carboxymethylation [15] and the so-called TEMPO-mediated oxidation [16].

Depending upon the cellulosic source and the process of production, MFC may have different dimensions, but it shows similar morphologies. As reported in Li et al. [6], MFC’s width can vary between 5 and 60 nm, while length is usually in the order of magnitude of micrometers. From these two characteristics derives a high aspect ratio, i.e. the ratio of the length to the width of the particle, an important parameter that determines the reinforcing properties of nanocellulose as a filler.

Another important characteristic that depends on both the source and the mechanical treatment of cellulosic fibers is the degree of crystallinity of MFC [6] [7]. As already mentioned, microfibrillated cellulose consists of both amorphous and crystalline regions and the degree of crystallinity determines many important properties of this material. For instance, the degree of crystallinity and the crystallite size affect the transparency, the tensile strength and the barrier properties of a polymer and each of these properties are essential for packaging application.

### 1.2.2 Nanopaper

Regardless of its morphology and its structural characteristics, MFC has shown an interesting film-forming capacity. MFC is usually obtained in water suspensions and when water is removed, a cellulose nanofiber network is formed thanks to interfibrillar hydrogen bonds. Indeed, the strong interactions between the microfibrils leads to the formation of MFC films which are sometimes called *nanopaper* [17].

In general, the starting suspension from which the films are obtained contains MFC in the range of 0,1-0,2 wt%, while the water removal can be reached through different processes. The main one consists of solvent casting and evaporation under controlled conditions of temperature and relative humidity [18]. Alternatively, MFC films can also be prepared through vacuum filtration [17] or using a dynamic sheet former [19]. An example of MFC nanopaper obtained by the solvent casting method is reported in **Figure 1.2**.

**Figure 1.2:** MFC nanopaper obtained by solvent casting method. With permission from *[18]*

MFC films produced through these processes have shown good barrier properties against oxygen, especially in dry condition [7]. Nevertheless, using these methods the film formation may take from several hours to days depending on the specific approach, which is unsuitable for a large-scale production. To speed up the process, Österberg et al. [20] proposed to prepare MFC films by pressurized filtration at 2,5 [bar] followed by a hot-pressing. After the first step of filtration, a 120 [µm] thick film was obtained in less than 30 minutes and the following hot-pressing took between 0,5 and 2 hours. All the films produced with this method showed very good oxygen barrier properties, even at a relative humidity of 65%.

A recent study managed to produce a nanopaper in less than 3 minutes. Usually, the fibrillation process is performed to obtain the nanocellulose and then the production of the film follows. In their work, Gorur et al. [21] inverted the order of the sequence. Firstly, they used classical papermaking methods to form a sheet of self-fibrillating fibers (SFF) prepared with a TEMPO and periodate oxidation and then a rapid in situ fibrillation was induced by a pH increase. Using this strategy, a sheet of dry thickness of 100 µm was obtained in less than 3 minutes: 10 s of dewatering time (thanks to conventional papermaking equipment) and 2 min for pH adjustment. After 12 min of an additional drying process, the nanopaper showed similar mechanical and barrier properties to those reported in the literature for nanopapers produced from MFC. This procedure has two important advantages from an industrial point of view: a high production speed and a minimum material loss.

### 1.2.3 Cellulosic nanocomposites

Although cellulose is a widespread and renewable resource, its application as a polymeric material is still rather limited. Among the open issues to be solved, the hydrophilic nature of MFC prevents its use at high relative humidity conditions. As well as causing high water vapor permeability, the interactions between the cellulosic material and the moisture worsen the barrier properties also against other gases such as oxygen [22]. In view of packaging application this is a drawback, although it guarantees easy degradation and composting.

A more promising use of MFC is its application as filler in composite materials, more specifically in nanocomposites. Nanocomposites can be defined as polyphasic materials in which the dispersed phase has at least one dimension in the nanometric range (1-100 nm).

Compared to traditional composites, nanocomposites show better mechanical and barrier properties even at low percentage of reinforcement (e.g., ≤5 wt%) [23].

As said before, cellulose is hydrophilic: this is a very important technological aspect to keep in mind when manufacturing cellulosic nanocomposites. This property affects the interactions between the polymer matrix and nanocellulose, thus influencing the degree of dispersion of the latter as a filler. Moreover, the formation of hydrogen bonds could cause the agglomeration of the dispersed phase and therefore compromise the properties of the nanocomposite.

Considering the compatibility between matrix and dispersed phase, MFC is particularly suitable to be used as filler in hydrophilic polymers such as polyvinyl alcohol (PVOH) or starch [24]. On the contrary, MFC cannot be uniformly dispersed in hydrophobic matrices as most polymeric materials are. Therefore, modifications are needed to improve compatibility with non-polar polymers.

Several strategies have been developed in order to improve the interactions between nanocellulose and hydrophobic polymers. One of them is to hydrophobize nanocellulose through chemical modification techniques that aim at modifying only the surface of the nanocellulose, while preserving its internal morphology characterized by a unique hydrogen-bond network.

Most surface modifications of nanocellulose are achieved by exploiting the reactivity of hydroxyl groups present on the monomer of cellulose, β-1,4-D-glucose. Among the several treatments developed to hydrophobize nanocellulose, surface acetylation of cellulose aims at substituting the hydroxyl groups of the fibers with acetyl groups that have a more hydrophobic nature [25]. Usually, it is performed using acetic acid or acetic anhydride under acid catalysis, as shown in the scheme reported in **Figure 1.3**. Acetylation with acetic anhydride was used to hydrophobize microfibrillated cellulose and obtain nanopapers with enhanced water vapor barrier properties [26].

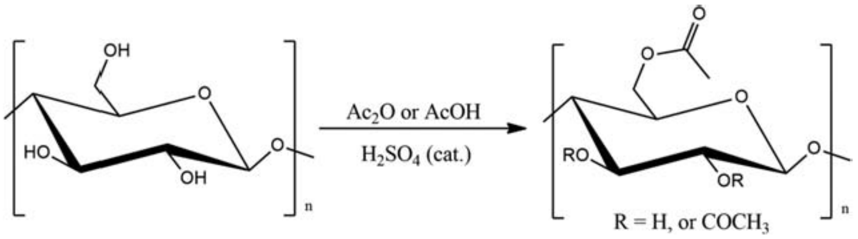

**Figure 1.3:** Reaction scheme of cellulose acetylation. With permission from *[25]*

Another strategy to improve the compatibility of nanocellulose with hydrophobic polymer is grafting it with apolar coupling agents. An example of this kind of modification was reported by Hassan et al. [27] who obtained a nanocomposite of polycaprolactone (PCL) reinforced with modified bagasse whiskers. In their work, cellulose whiskers were modified with n-octadecyl isocyanate and after this process no agglomeration within the nanocomposite film occurred. Moreover, thanks to the good distribution of whisker in the PCL matrix, nanocomposites showed higher moisture-barrier properties with respect to neat PCL film.

Another approach to obtain nanocomposites made of an apolar matrix and nanocellulose was studied by Ljungberg et al. [28]. Using surfactants, they managed to get a stable dispersion of cellulose whiskers in a nonpolar solvent, i.e. toluene. By mixing this dispersion with solubilized atactic polypropylene in hot toluene and after solvent evaporation, they produced a nanocomposites film where cellulose whiskers were finely dispersed in the polymer matrix, as demonstrated by the transparency of the film.

Depending on the type of polymeric matrix chosen to be reinforced with MFC, these modifications may or may not be necessary. As regards the manufacturing of cellulosic nanocomposites, there are many methods that have been discussed in the literature. The most promising ones are the solvent/solution casting method, the melt intercalation process, the in-situ polymerization and the coating technique [9].

The nanocomposite studied in this work consists of a biobased latex reinforced with MFC. Other latex composites reinforced with nanocellulose have been reported in literature. Bacterial Cellulose has been used as filler in natural rubber latex via an aqueous microdispersion process [29]. In another study, natural rubber latex has been reinforced with nitro-oxidized cellulose nanofibers [30]. In both cases, reinforcement by nanocellulosic fillers improved the mechanical properties of the latex, while barrier properties were not examined.

Gas transport through nano and micro composite of latexes has been investigated by introducing different kind of fillers into natural rubber, carboxylated styrene butadiene rubber and their blends. Layered silicates were used as nanofillers, while clay and silica were employed for the preparation of microcomposites. Nanocomposites exhibited a higher improvement in barrier properties towards oxygen and nitrogen with respect to microcoposites [31]. Another latex nanocomposite with enhanced oxygen barrier properties has been obtained by incorporating surface-modified graphene oxide into a styrene-acrylic latex [32].

## *1.3 Permeability*

### 1.3.1 Packaging and barrier properties

Packaging has been defined as "*a socio-scientific discipline which operates in society to ensure delivery of goods to the ultimate consumer of those goods in the best condition intended for their use*" (Lockhart, 1997) [33]. This multidisciplinary role of packaging reflects in its four main functions: containment, protection, convenience and communication [34].

The most straightforward task is that of containment, fundamental for all those products that do not have their own shape, such has fluids or powder. Another important function is the protection of the goods, which is particularly essential for the preservation of foodstuff. Indeed, today's food packaging technologies are meant to protect the product from mechanical stress and external agents such as moisture, microorganisms and dust. Finally, the other two functions are more related to package design and consumer marketing. Convenient packages aim at meeting the demands of consumer, making the product easier to use. An example of this kind of service may be easy opening packages or containers that allow the cooking of the product directly in the package. In the end, there is the communication function, that is as important as the others: in addition to the advertising role, package must communicate information that must be provided to consumers by law.

Among all the functions mentioned above, perhaps the most relevant is the protection and preservation of the product. Packaging performs this task acting as a barrier between the inside and outside of the package. This action takes place in both directions: from one side it prevents external agents from entering, but also prevents the leakage of internal compounds such as aroma. Both of these aspects are essential for the preservation of a food product for instance.

The barrier properties of plastics are therefore essential as they prevent or slow down the transport of gases and vapors through the package. Among the main external agents that could compromise the conservation of the product there are oxygen and water vapor. The former may cause rancidity phenomena in some foodstuff, while the latter, in the form of moisture in the air, may provoke the softening of dry products or the formation of moulds. Nevertheless, it is important not to underestimate the transport of gas from the inside to the outside. Many food products are stored in the so-called Modified Atmosphere Packaging (MAP) in which the composition of the atmosphere has been specially designed to improve conservation. Therefore, it is essential that packaging prevents the leakage of this kind of atmosphere, or, to take another example, $CO_2$ leakage from carbonated drinks.

### 1.3.2 Gas and vapor permeation

The main processes by which gas and vapor can pass through a polymeric packaging are essentially two [34]:

- Capillary flows: the gases pass through microscopic channels or cracks in the package. This mechanism depends on the integrity of the packaging.
- Permeation: this phenomenon takes place even if the packaging is intact and it occurs because gas (vapor) permeates the inter/intra-molecular free volume of the polymer.

The latter process of mass transport concerns low molecular weight gases and liquids and it consists of three steps:

1. Adsorption: the permeant molecule dissolves at one surface of the polymer following Henry's law (1.1).

$$c = S \cdot p \tag{1.1}$$

where: $c$ is the concentration of the dissolved permeant.

$S$ is the solubility coefficient of the permeant in the polymer.

$p$ is the partial pressure of the permeant at equilibrium with the polymer.

2. Diffusion: the permeant diffuses through the polymer according to Fick's first law (1.2).

$$F = -D\frac{\partial c}{\partial x} \tag{1.2}$$

where: $F$ is the flux per unit area of permeant through the polymer.

$D$ is the diffusion coefficient.

$\frac{\partial c}{\partial x}$ is the concentration gradient of the permeant.

3. Desorption: the permeant evaporates at the other surface of the polymer, always following Henry's law (1.1).

All these three mechanisms are schematically represented in **Figure 1.4** where a one-dimensional polymer film of thickness $L$ and area $A$ is considered. This film is exposed to a generic permeant at pressure $p_1$ on one side and at lower pressure $p_2$ on the other. The permeant molecule dissolves at the polymer interface and diffuses through the film thickness by virtue of the concentration gradient that is generated between the two sides of the film.

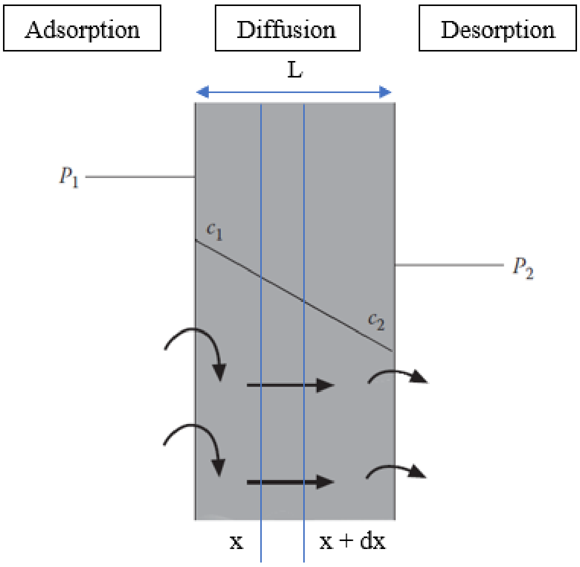

**Figure 1.4:** Permeation of gas and vapor through a polymeric film. Adapted from *[34]*

A balance on permeant is made over a control volume consisting of a layer of polymer with infinitesimal thickness $dx$. This mass balance leads to Equation (1.3):

$$A \cdot F|_x = A \cdot F|_{x+dx} + \frac{\partial c}{\partial t} \cdot A \cdot dx \tag{1.3}$$

Simplifying the expression,

$$\frac{\partial c}{\partial t} = -\frac{\partial F}{\partial x} \tag{1.4}$$

By combining Equation (1.4) and Fick's first law (1.2), a simplified form of the so-called Fick's second law is obtained (1.5).

$$\frac{\partial c}{\partial t} = D\frac{\partial^2 c}{\partial x^2} \tag{1.5}$$

At steady-state conditions, the concentration derivative with respect to time is cancelled and it can be demonstrated that the permeant flux is constant. Equation (1.2) can be integrated across the total thickness of the polymer $L$ and between the two concentrations, assuming the diffusion coefficient to be constant and independent of concentration. An alternative expression of the flux can thus be obtained:

$$F = D\frac{c_1 - c_2}{L} \tag{1.6}$$

By applying Henry's law (1.1), concentration in Equation (1.6) can be expressed in relation to solubility and partial pressure of the permeant. Doing so, Equation (1.7) is obtained.

$$F = DS\frac{p_1 - p_2}{L} \tag{1.7}$$

The product between the diffusion coefficient and the solubility coefficient is referred to as the *permeability coefficient* (or *constant*) and is represented by the symbol $K_P$. Definition is given in Equation (1.8).

$$K_P = D \cdot S \tag{1.8}$$

By defining the flux of permeant as the amount of permeant $q$ passing through surface $A$ in the time unit, an alternative expression of $F$ is given in Equation (1.9):

$$F = \frac{q}{A \cdot t} \tag{1.9}$$

Replacing Equations (1.9) and (1.8) in Equation (1.7), a new equation is obtained:

$$\frac{q}{A \cdot t} = K_P\frac{p_1 - p_2}{L} \tag{1.10}$$

From the latter equation, the permeability coefficient finds an alternative definition given in Equation (1.11).

$$K_P = \frac{q \cdot L}{A \cdot t(p_1 - p_2)} \tag{1.11}$$

The permeability coefficient $K_P$ is therefore the amount of gas $q$ that permeates a film of thickness $L$ and area $A$ in the time unit by the effect of a driving force represented by the difference in pressure of the permeant between the two faces of the film. All the mathematical steps written above are taken from Robertson [34].

In the literature there exist other parameters that describe the phenomenon of permeation. One of them is the *Gas Transmission Rate (GTR),* defined as follows:

$$GTR = \frac{q}{A \cdot t} \tag{1.12}$$

The relationship between $GTR$ and $K_P$ is given by Equation (1.13).

$$GTR = \frac{K_P}{L}\Delta p \tag{1.13}$$

Where $\Delta p$ is the gradient of pressure ($p_1$-$p_2$) between the two sides of a polymer film of thickness $L$.

Another parameter that can be found in the literature is the *permeance P,* which can be related to the permeability coefficient $K_P$ as follows:

$$P = \frac{K_P}{L} \tag{1.14}$$

Regardless of the parameter used for its description, the permeation process is regulated by the adsorption of the permeant and its diffusion through the polymeric material. During adsorption, the permeant molecules occupy the free volume holes of the polymer that are created by thermal agitation or by Brownian motions of the chains. As a consequence of chains mobility, these voids within the free volume of the polymer are generated and move within the polymeric material and diffusion occurs by jumps through neighboring holes [35].

In semicrystalline polymers, one of the factors affecting permeability is the crystalline content. In fact, it is assumed that free volume is only available in amorphous regions while the crystallites are impermeable to gas molecules. Therefore, the higher the degree of crystallinity of a polymer, the lower its permeability. As reported in Equation (1.8), the permeability coefficient is defined as the product between solubility and diffusion coefficients of the permeant; the degree of crystallinity affects both of these factors.

For semicrystalline polymers, the solubility coefficient $S$ can be expressed as a function of the volume fraction of the crystalline phase $\phi_c$ by the following expression:

$$S = S_0(1 - \phi_c) \tag{1.15}$$

where $S_0$ is the solubility coefficient of the amorphous phase [35].

Concerning the diffusion process, the crystalline domains have two different effects on it. Since the crystallites are impermeable to gas molecules, their presence forces permeant molecules to follow longer path. This effect is expressed by the *tortuosity factor* $\tau$: the higher the tortuosity, the longer it will take the gas to diffuse within the polymeric material. Another aspect to consider is that crystals share polymer chains with amorphous regions, thus reducing their mobility and so the free volume. This second effect is taken into account by introducing the *chain immobilization factor* $\beta$. With consideration for both $\tau$ and $\beta$, the diffusion coefficient $D$ for a semicrystalline polymer can be expressed as the ratio reported in Equation (1.16).

$$D = \frac{D_0}{\beta\tau} \tag{1.16}$$

Where $D_0$ is the diffusion coefficient for fully amorphous polymer. Since both $\tau$ and $\beta$ are greater than 1, the actual diffusion coefficient $D$ is lower than $D_0$ [35].

### 1.3.3 Permeability tests

There are several experimental methods to evaluate the barrier properties of a material. In the main one, a cell is divided into two chambers by the polymer film under examination and the passage of a test gas through the film is studied. During the experiment, a gas flow of known composition is sent in the upper chamber delimited by the polymer film. As shown in Equation (1.11), the passage of the permeant is governed by the difference in its partial pressure between the two faces of the film. This gradient of pressure can be provided with two main different approaches [36]:

- Integral mode: the lower chamber is under vacuum condition and the cumulative amount $q$ of the permeant passed through the film is measured.
- Differential mode: a gas carrier flow that does not contain the permeant is sent in the lower chamber and the flow $J$ of the permeant that passes through the film is measured at the outlet of the lower chamber.

A schematic representation of the experimental cells for of the gas permeability test recommended for these methods is reported in **Figure 1.5**.

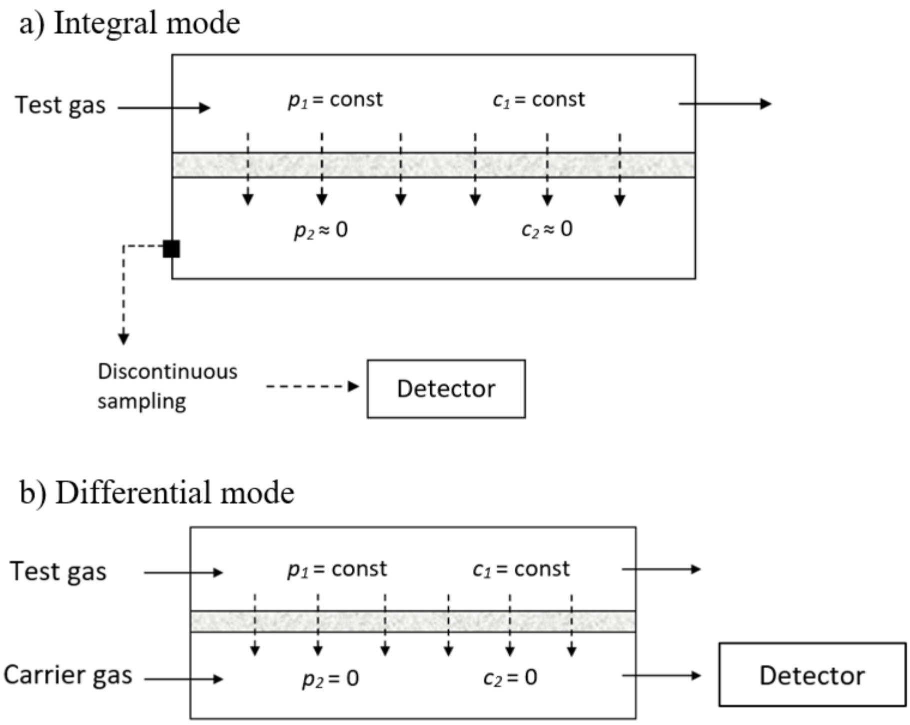

**Figure 1.5:** Schemes of the experimental cell for gas permeability test

As already proved in Eq. (1.5), one-dimensional diffusion in a polymeric film of thickness $L$ is described by the second Fick's law (1.17):

$$\frac{\partial c(x,t)}{\partial t} = D\frac{\partial^2 c(x,t)}{\partial x^2} \tag{1.17}$$

The 1D solution applicable in the experiments described above is subjected to the following condition. The boundary conditions on both sides of the film are given by Eq. (1.18):

$$\begin{cases} c(0,t) = c_1 \\ c(L,t) = 0 \end{cases} \tag{1.18}$$

In addition to these boundary condition, there is also an initial condition given by Eq. (1.19):

$$c(x,0) = 0 \tag{1.19}$$

Here, *c(x,t)* describes how the permeant concentration of the permeant changes with time within the film. In the boundary conditions, $c_1$ is the concentration of the permeant in the upper chamber of the cell, which is fixed by the composition of the test gas. Instead, in the lower chamber $c_2 = 0$ both in the integral mode and in the differential mode. In the former case, the lower chamber is under vacuum condition and the concentration of the permeant increases as it accumulates, but for short times one can assume $c_2 \approx 0$ so that the pressure gradient can be considered as constant. In the differential method, the concentration of the permeant in the lower chamber is zero as the carrier gas does not contain it, so the pressure gradient is always constant.

Theoretical kinetic curves for these methods of the gas permeability test are shown in **Figure 1.6**.

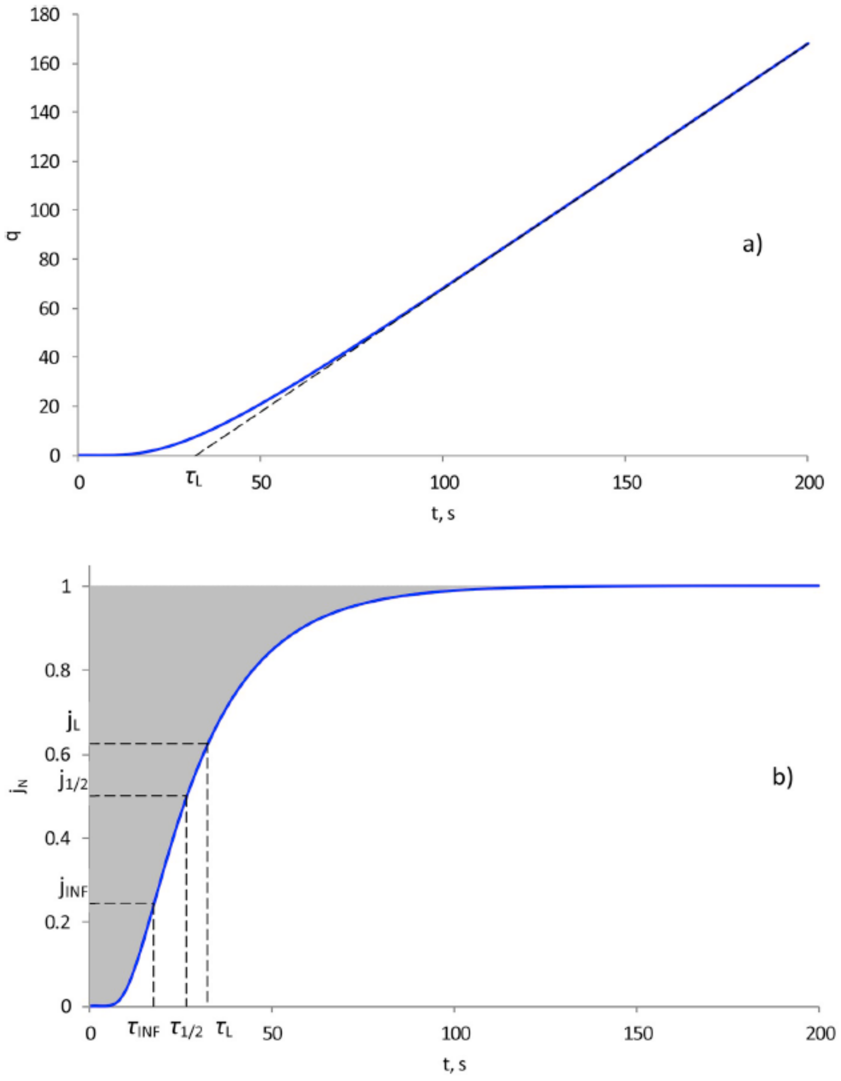

**Figure 1.6:**Theoretical kinetic curves of different methods of permeability test: (a) integral mode (b) differential mode. The shaded area in (b) is equal to the first moment $\mu_1$. With permission from *[36]*

*Integral method*

In the integral mode of the gas permeability test, the amount of permeant passing through the film *q(t)* is recorded. For classical diffusion, the time dependance is given by the expression in Eq. (1.20) [36].

$$q(t) = Ac_1\left\{\frac{D}{L}t + \frac{2L}{\pi^2}\sum_{n=1}^{\infty}\frac{(-1)^n}{n^2}\left[1 - \exp\left(-\frac{Dn^2\pi^2t}{L^2}\right)\right]\right\} \tag{1.20}$$

Where $D$ is the diffusion coefficient of the permeant gas in the polymer and $L$ is the thickness of the polymer film under examination.

As shown in **Figure 1.6a** at large time the curve of the amount of permeant becomes a straight line. Indeed, for larger times the dependence can be approximated linearly with the expression given in Eq. (1.21) [36]:

$$q(t) = \frac{Ac_1D}{L}\left(t - \frac{L^2}{6D}\right) \tag{1.21}$$

By replacing the concentration with the Henry's law (1.1) and remembering that the product of the diffusion coefficient $D$ and the solubility $S$ gives permeability coefficient $K_P$ (1.8), the linear expression of *q(t)* can be rewritten as follows:

$$q(t) = \frac{AK_Pp_1}{L}\left(t - \frac{L^2}{6D}\right) \tag{1.22}$$

Extrapolating this line, one can derive several parameters. For example, the slope of the line allows to evaluate the permeability coefficient $K_P$ of the polymer film. Moreover, as shown in **Figure 1.6a**, the straight line cuts the abscissa axis at a point called *time-lag* $\tau_L$. After calculating the interception with the time axis, one can evaluate the time-lag and derive the diffusion coefficient by using Equation (1.23).

$$D = \frac{L^2}{6\tau_L} \tag{1.23}$$

This procedure for the estimation of the gas diffusion coefficient in the polymer is called *time-lag method.*

*Differential method*

In the differential mode, the flow of permeant at the outlet of the lower chamber over time *J(t)* is measured. In case of the boundary condition given in Eq. (1.18), the time dependence of the flow is given by Equation (1.24) [36].

$$J(t) = \frac{Ac_1D}{L}\left[1 + 2\sum_{n=1}^{\infty}(-1)^n exp\left(-\frac{n^2\pi^2}{L^2}Dt\right)\right] \tag{1.24}$$

After long time, i.e. at t→∞, a steady-state diffusion flow $J_\infty$ is reached, which is equal to the expression in Equation (1.25) [36].

$$J_\infty = \frac{Ac_1D}{L} \tag{1.25}$$

As already done for Equation (1.21), the expression of the asymptotic value of the flow can be rewritten as follows:

$$J_\infty = \frac{AK_Pp_1}{L} \tag{1.26}$$

In the end, from the stationary flow given in Eq. (1.26) it is possible to evaluate the permeability coefficient $K_P$.

For what concerns the estimation of the diffusion coefficient, there are different methods to process the experimental data obtained by the differential mode. Singular points method and statistical moments method are two of the main procedures. Both of them needs normalization of the kinetic curve with respect to the stationary flow. By introducing the normalized flow $j_N$, given by Eq. (1.27), it is possible to obtain the curve shown in **Figure 1.6b.**

$$j_N = \frac{J(t)}{J_\infty} \tag{1.27}$$

The easiest methods for the estimation of the diffusion coefficient are based on the evaluation of singular points on the differential kinetic curve. One of the singular points methods described in Beckman et al. [36] consists in identifying the so called *half time* $\tau_{1/2}$ which is the time required for the flow $J$ to reach half of its stationary value $J_\infty$ (in terms of $j_N$ it is the time required to reach the value of 0,5). After the evaluation of this point from the experimental curve, the diffusion coefficient $D$ can be evaluated by the expression given in Eq. (1.28) [36].

$$D = \frac{L^2}{7{,}2\tau_{1/2}} \tag{1.28}$$

Another singular point that can be identified on the differential kinetic curve is the *inflection point time* $\tau_{INF}$. The expression for the estimation of $D$ from $\tau_{INF}$ is given in Beckman et al. [36].

In addition to the singular points methods, the statistical moments method is another technique for the estimation of the gas diffusion coefficient in the polymer. The procedure for the elaboration of the experimental data obtained with the differential mode was given by Felder [37]. The moment method consists of the calculation of the moment $\mu_1$ defined as follows:

$$\mu_1 = \int_0^\infty (1 - j_N)dt \tag{1.29}$$

This integral can be performed by numerical integration of the experimental curve evaluated with the differential mode. It can be demonstrated that the moment $\mu_1$ coincides with the time-lag $\tau_L$ evaluated in the integral mode curve [37].

Indeed, the quantities experimentally measured in the integral mode and in the differential mode are correlated with Equation (1.30) [37].

$$q(t) = \int_0^t J(t')dt' \tag{1.30}$$

As already seen in Eq. (1.22), the plot of $q$ vs. $t$ obtained through the integral mode approaches a straight line for larger time. The slope of this line is equal to the stationary flow $J_\infty$ measured in the differential mode (1.26). Therefore, the linear time dependance of *q(t)* can be rewritten as follows:

$$q(t) = J_\infty(t - \tau_L) + h(t) \tag{1.31}$$

Where $\tau_L$ is the time-lag and *h(t)* is the difference between the exact function *q(t)* and its asymptotic limit [37]. By definition

$$\lim_{t\to\infty} h(t) = 0 \tag{1.32}$$

The moment $\mu_1$ of Equation (1.29) may can be written as:

$$\mu_1 = \lim_{t\to\infty} \int_0^t (1 - j_N)dt' \tag{1.33}$$

Or

$$\mu_1 = \lim_{t\to\infty} \left(t - \frac{1}{J_\infty}\int_0^t J(t')dt'\right) \tag{1.34}$$

For Equation (1.30), the integral in Eq. (1.34) is equal to *q(t)*.

$$\mu_1 = \lim_{t\to\infty} \left[t - \frac{q(t)}{J_\infty}\right] \tag{1.35}$$

By substituting *q(t)* with the expression in Eq. (1.31):

$$\mu_1 = \lim_{t\to\infty}\left[t - (t - \tau_L) - \frac{h(t)}{J_\infty}\right] \tag{1.36}$$

Simplifying the expression,

$$\mu_1 = \tau_L - \frac{1}{J_\infty}\lim_{t\to\infty} h(t) \tag{1.37}$$

From Equation (1.32), the following equality is demonstrated:

$$\mu_1 = \tau_L \tag{1.38}$$

Given this correlation, it is possible to estimate the diffusion coefficient *D* using a modified version of Equation (1.28):

$$D = \frac{L^2}{6\mu_1} \tag{1.39}$$

Where the moment $\mu_1$ can be evaluated through numerical integration of Equation (1.29).

### 1.3.4 Permeability of nanocomposites

There exist various strategies through which it is possible to improve the barrier properties of a polymeric system. Basically, permeability control can be achieved by incorporating a secondary phase with the purpose to increase the tortuosity of the diffusion path. This strategy can be implemented by developing polymer blends, polymer composites or nanocomposites or polymer foams [38].

In a polymer blend, the dispersed phase consists of a second polymer with different properties with respect to the matrix. Composites are instead multi-phase systems with fillers distributed in a polymer matrix. When these fillers have at least one dimension in the nanoscale, the system is referred to as nanocomposite. Finally, polymer foams are porous materials with a continuous polymeric phase and a discontinuous gaseous phase [38].

In this work, the strategy adopted to improve barrier properties consists in dispersing cellulosic fillers in a polymer matrix. The incorporation of fillers causes a reduction in permeability due to two aspects. First, there is a decrease in solubility due to the nanofillers reducing the polymer matrix volume. In addition to this, the presence of nanofillers increases the tortuosity of the diffusive path, as shown in **Figure 1.7**.

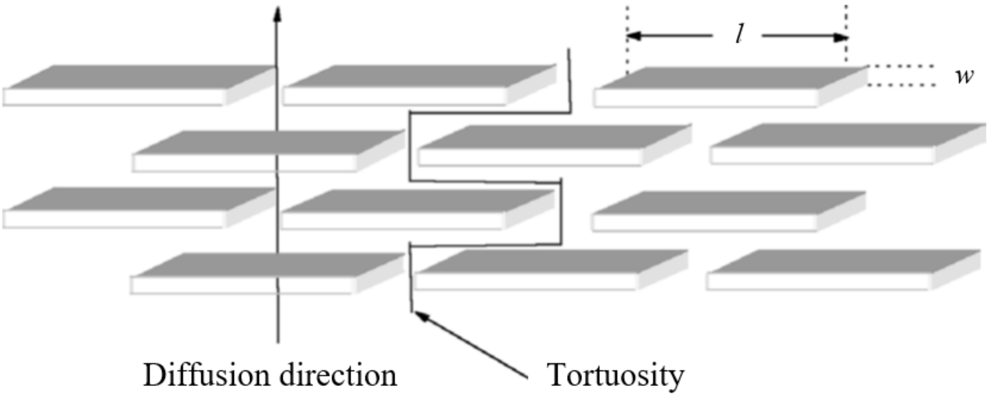

**Figure 1.7:** Increasing of tortuosity due to incorporation of nanofillers. Adapted from *[35]*

Since in most common nanocomposites the fraction of nanofillers is usually low, the reduction of the matrix volume is small and so is the decrease of the solubility. Therefore, the predominant effect is the reduction of the diffusion coefficient due to the increased tortuosity of the path [35].

In addition to the volume fraction of the nanofillers $\phi$, there are two other main factors that influence the permeability of a nanocomposites: the orientation of the fillers with respect to the diffusion direction and their aspect ratio [35]. With reference to **Figure 1.7**, the aspect ratio $\alpha$ can be defined as the ratio between the length $l$ and the width $w$ of the nanofillers.

$$\alpha = \frac{l}{w} \tag{1.40}$$

As reported in Choudalakis and Gotsis [35], the tortuosity factor $\tau$ of a nanocomposite can be expressed as a function of the volume fraction of the fillers $\phi$ and their aspect ratio $\alpha$. This relationship is presented in Equation (1.41).

$$\tau = 1 + \frac{\alpha}{2}\phi \tag{1.41}$$

Nanofillers with high aspect ratio cause a significant increase of the tortuosity, thus enhancing the barrier properties of the nanocomposites.

For what concerns the orientation of the fillers, depending on their dispersion in the polymer matrix, three types of composites can be obtained: tactoid, intercalated and exfoliated structures [39]. These three different morphologies are represented in **Figure 1.8**.

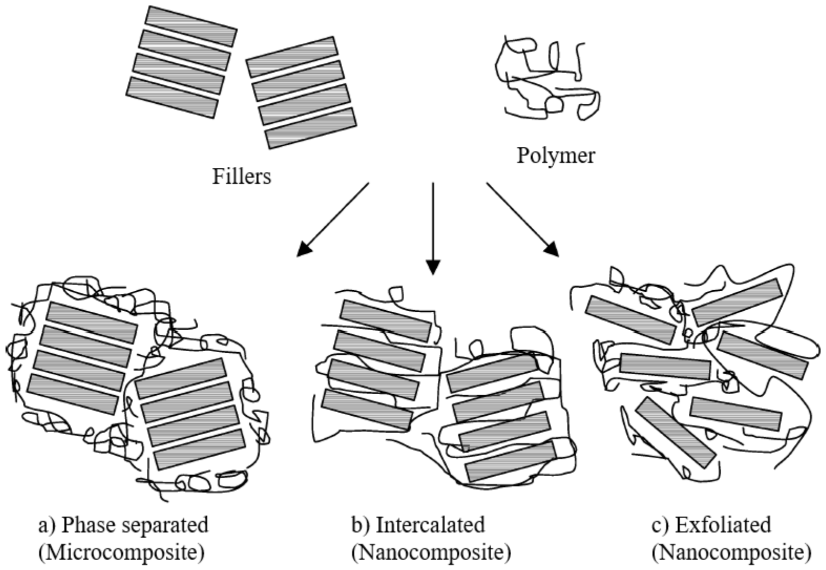

**Figure 1.8**: Types of composite structures: a) tactoid, b) intercalated and c) exfoliated morphologies. Adapted from *[39]*

Tactoid configuration occurs when the fillers are not well dispersed and the system obtained is referred to as microcomposite. A possible cause of this structure may be a weak interfacial adhesion between fillers and polymer matrix. As a consequence of this, aggregation of the nanofillers occurs and aspect ratio decreases as well. This situation should be avoided because it may not give the desired effect on the decrease of permeability.

Conversely, intercalation and exfoliation produce ideal nanocomposites. With respect to the intercalated nanocomposite, the fully exfoliated one shows much higher values for the tortuosity factor and the aspect ratio and so it is much more effective to enhance the barrier properties of the nanocomposite [35].

As already mentioned in the treatment of cellulosic nanocomposites, the hydrophilicity of MFC affects its degree of dispersion in a polymer matrix. Without a suitable interfacial adhesion between the dispersed and continuous phases, the presence of nanofibers within the polymer may lead to the creation of a preferential pathway for the diffusion of the permeant at the filler/matrix interface and the formation of microscopic holes in the matrix [38]. Both of these outcomes may result in increased permeability, thus making the incorporation of nanocellulose counterproductive to improve barrier properties.

Therefore, it is crucial to enhance the interfacial adhesion between the nanocellulose and the matrix, especially when the latter consists of an apolar polymer. The main methods to improve this property have been already mentioned when cellulosic nanocomposites were introduced. Interfacial adhesion is an essential factor in controlling the barrier properties of the nanocomposite and so it is important to choose the proper modification technique according to the nature of the polymer matrix.

### 1.3.5 Permeability of cellulosic nanomaterials

The plastics mainly adopted in the packaging industry are synthetic polymers such as polyethylene (PE), polypropylene (PP), polyvinyl alcohol (PVOH) or polystyrene (PS). All these materials have a petrochemical origin and are characterized by a low production cost. Although these materials have properties that make them ideal for packaging application, they do not meet the sustainability criteria sought in our days.

Given the growing awareness of environmental issues related to the use of traditional plastics, scientific research in recent years has focused on the study of new sustainable materials able to compete with petroleum-based polymers. Biobased polymers, i.e. organic materials whose atomic carbon comes from renewable resources, are a viable alternative to synthetic polymers. A type of bio-based materials consists of polymers extracted from natural resources and cellulose belongs to this class. Considering the packaging field, nanocellulose offers very promising prospect and several studies have been done to evaluate its properties.

In this context, both microfibrillated cellulose MFC and cellulose nanocrystals CNC have been investigated to develop self-standing film with good barrier properties. **Table 1.1** presents a review of the permeability towards oxygen of different nanopapers found in the literature. Data are reported either in terms of permeability coefficient towards oxygen, denoted as $O_2$ Permeability (OP), or in terms of Oxygen Transmission Rate (OTR). In most cases, nanopapers have shown high barrier properties, suitable for instance for application in modified atmosphere packaging (MAP). The recommended values of OTR for MAP application are below 10-20 [cc $m^{-2}$ $day^{-1}$] [26] and the majority of the developed films meet this condition.

While nanopapers have excellent barrier properties against oxygen, permeability towards water vapor is not as good. In this regard, several data found in the literature are presented in **Table 1.2**. A 25 μm thick film of low density polyethylene (LDPE), one of the most common packaging materials, has a Water Vapor Transmission Rate (WVTR) of 4 [g $m^{-2}$ $day^{-1}$] [34]. By making a comparison with it, all the nanopapers that have been reported have shown higher values of WVTR. These poor barrier properties against water vapor prevent nanopapers from being used as packaging material in different applications.

As already mentioned when cellulosic nanocomposites were introduced, the most promising application of nanocellulose is its use as filler. The barrier properties of several materials reinforced with nanocellulose have been studied. **Table 1.3** presents the permeation properties towards oxygen, while **Table 1.4** shows the permeability data towards water vapor. In both of the tables, the content of nanocellulose is reported either as weight percentage or as the thickness of the layer applied in the coating technique. All nanocomposites examined show an improvement in barrier properties as the nanocellulose content increases.

**Table 1.1:** Barrier properties of nanopapers against oxygen

| Source of cellulose | Fibrillation method | Type of nanocellulose | Nanopaper production | T [°C] | RH [%] | OTR [cc/m$^2$ d] | $O_2$ Permeability [cc µm/m$^2$ d kPa] | Ref. |
|---|---|---|---|---|---|---|---|---|
| Sulfite softwood dissolving pulp | Carboxymethylation + homogenization | MFC | Solvent casting | 23 | 50 |  | 0,36 | [18] |
| Bleached spruce sulphite pulp | Homogenization | MFC | Solvent casting | 23 | 50 | $20,4^b$ |  | [19] |
| Kraft pulp from Norway spruce | Refining + homogenization | MFC | Solvent casting | 23 | 0 | 4,2 | $0,80^a$ | [26] |
| Bleached softwood kraft pulp | Refining | MFC | Solvent casting | 25 | 50 | $1,7^b$ |  | [40] |
|  | Refining + grinding | MFC | Solvent casting | 25 | 50 | $1,4^b$ |  |  |
| Hardwood bleached eucalyptus kraft pulp | TEMPO-oxidation + homogenization | TOCN | Solvent casting | 25 | 50 | $3,7^b$ |  |  |
| Softwood conifer bleached kraft pulp | TEMPO-oxidation + homogenization | TOCN | Solvent casting | 25 | 50 | $6^b$ |  |  |
| Bleached softwood kraft pulp | Sonication | MFC | Vacuum filtration | 23 | 0 | $11963,69^b$ |  | [41] |
|  |  |  | + hot pressing | 23 | 0 | $10,25^b$ |  |  |
|  |  |  |  | 23 | 90 | $59,25^b$ |  |  |

**Table 1.1:** (continued)

| **Source of cellulose** | **Fibrillation method** | **Type of nanocellulose** | **Nanopaper production** | **T [°C]** | **RH [%]** | **OTR [cc/m² d]** | **O₂ Permeability [cc µm/m² d kPa]** | **Ref.** |
|---|---|---|---|---|---|---|---|---|
| - | TEMPO-oxidation + homogenization | TOCN | Vacuum filtration | 23 | 50 | | 0,203 | [42] |
| | | | | 23 | 80 | | ~ 1,5 | |
| | | | + oven heating at 145 °cC | 23 | 50 | | 0,007 | |
| | | | | 23 | 80 | | 0,584 | |
| Dissolving pulp | Sulfuric acid hydrolysis | CNC | Solvent casting | 23 | 80 | 55,2 | 20 | [43] |
| Bleached northern softwood kraft pulp | Disk refining | MFC | Solvent casting | 23 | 80 | 31,8 | 11,1 | |
| Bleached kraft wood pulp | TEMPO-oxidation + homogenization | TOCN | Solvent casting | 23 | 85 | 83,8 | ~ 30 | [44] |

a. Calculated from the OTR following the reference standard.
b. OTR values normalized to 25 [µm] thickness.

Table 1.2: Barrier properties of nanopapers against water vapor

| Source of cellulose | Fibrillation method | Type of nanocellulose | Nanopaper production | Thickness [µm] | T [°C] | RH [%] | WVTR [g/$m^2$ d] | Ref. |
|---|---|---|---|---|---|---|---|---|
| Kraft pulp from Norway spruce | Refining + homogenization | MFC | Solvent casting | 42 | 23 °C | 50 | 234 | [26] |
|  | + heterogeneous acetylation |  |  | 46 | 23 °C | 50 | 167 |  |
| Bleached softwood kraft pulp | Refining | MFC | Solvent casting | 25 | 25 °C | 50 | 52 | [40] |
|  | Refining + grinding | MFC | Solvent casting | 25 | 25 °C | 50 | 51 |  |
| Hardwood bleached eucalyptus kraft pulp | TEMPO-oxidation + homogenization | CNC | Solvent casting | 25 | 25 °C | 50 | 162 |  |
| Softwood conifer bleached kraft pulp | TEMPO-oxidation + homogenization | CNC | Solvent casting | 25 | 25 °C | 50 | 181 |  |
| - | TEMPO-oxidation + homogenization | TOCN | Vacuum filtration | 16 | 23 | 50 | ~ 115 | [42] |
|  |  |  | + oven heating at 145 °cC | 16 | 23 | 50 | 12,3 |  |

**Table 1.2:** (continued)

| Source of cellulose | Fibrillation method | Type of nanocellulose | Nanopaper production | Thickness [µm] | T [°C] | RH [%] | WVTR [g/m$^2$ d] | Ref. |
|---|---|---|---|---|---|---|---|---|
| Dissolving pulp | Sulfuric acid hydrolysis | CNC | Solvent casting | 36 | 23 | 50 | 452 | [43] |
| Bleached northern softwood kraft pulp | Disk refining | MFC | Solvent casting | 39 | 23 | 50 | 407,6 | |
| Bleached kraft wood pulp | TEMPO-oxidation + homogenization | TOCN | Solvent casting | 29,8 | 23 | 50 | 276,6 | [44] |

**Table 1.3:** Barrier properties of cellulosic nanocomposites against oxygen. OTR is expressed in [cc/(m$^2$ d)]. OP is expressed in [cc µm/(m$^2$ d kPa)]

| Source of cellulose | Type of nanocellulose | Matrix | Nanocomposite production | Cellulose wt% | T [°C] | RH [%] | OTR | OP | Ref. |
|---|---|---|---|---|---|---|---|---|---|
| Bleached sulfite softwood pulp | MFC | Amylopectin | Coating | 15 | 23 | 50 | | 0,365 | [45] |
| | | | | 50 | 23 | 50 | | 0,197 | |
| Sulfite softwood dissolving pulp | MFC | Amylopectin | Coating | 15 | 23 | 50 | | 0,335 | |
| | | | | 50 | 23 | 50 | | 0,128 | |
| - | CNC | PLA | Solution casting | 0 | 24 | 80 | | 1183,68 | [46] |
| | | | | 5 | 24 | 80 | | 129,6 | |
| Norway spruce | TOCN | PET | Coating | 0 | 23 | 0 | 29,3 | 14,46$^c$ | [47] |
| | | | | 1 µm | 23 | 0 | 0,08 | 0,04$^c$ | |
| Eucalyptus pulp | TOCN | PET | Coating | 0 | 23 | 0 | 29,3 | 14,46$^c$ | |
| | | | | 1 µm | 23 | 0 | 1,09 | 0,55$^c$ | |

**Table 1.3:** (continued)

| **Source of cellulose** | **Type of nanocellulose** | **Matrix** | **Nanocomposite production** | **Cellulose wt%** | **T [°C]** | **RH [%]** | **OTR** | **OP** | **Ref.** |
|---|---|---|---|---|---|---|---|---|---|
| Never-dried softwood bleached kraft pulp | TOCN | PET | Coating | 0 | 23 | 0 | | 15,5 | [48] |
| | | | | 1 µm | 23 | 0 | | 0,0017 | |
| Hardwood kraft pulp | MFC | PET | Coating | 0 | room T | 0 | 46,69 | 23,04 | [49] |
| | | | | ~ 2 µm | room T | 0 | 2,56 | 1,32 | |

c. Calculated from the OTR following the reference standard.

**Table 1.4:** Barrier properties of cellulosic nanocomposites against water vapor. Water Vapor Permeability coefficient (WVP) is expressed in [g µm/(m$^2$ d kPa)]

| Source of cellulose | Type of nanocellulose | Matrix | Nanocomposite production | Cellulose wt% | T [°C] | RH [%] | WVP | Ref. |
|---|---|---|---|---|---|---|---|---|
| Sugar palm | CNC | Sugar palm starch |  | 0 | 25 | 75 | 82771 | [24] |
|  |  |  |  | ~ 0,5 | 25 | 75 | 66266 |  |
| - | CNC | PLA | Solution casting | 0 | 24 | 75 | 1989,79 | [46] |
|  |  |  |  | 3 | 24 | 75 | 364,61 |  |
| - | CNC | Carrageenan | Solution casting | 0 | 24 | 75 | 5927 | [50] |
|  |  |  |  | 3 | 24 | 75 | 1736 |  |
| - | CNC | Mango puree | Solution casting | 0 | 25 | - | 63840 | [51] |
|  |  |  |  | 36 | 25 | - | 40080 |  |
| - | CNC | Chitosan | Solution casting | 0 | 25 | - | 17290 | [52] |
|  |  |  |  | 10 | 25 | - | 14110 |  |

# 2. Experimental

## *2.1 Materials*

In this work, microfibrillated cellulose Exilva 01-V (shortened with EV) provided by Borregaard (Norway) was used. MFC has a concentration of 10% wt in water and looks like a very viscous white paste.

The polymer matrix used consists of a biobased latex produced from eugenol-based methacrylate, more precisely from Ethoxy Dihydroeugenyl Methacrylate (EDMA), whose structure is reported in **Figure 2.1**. For the first part of this study, a latex with 15% of Total Solid Content (TSC) of EDMA has been used.

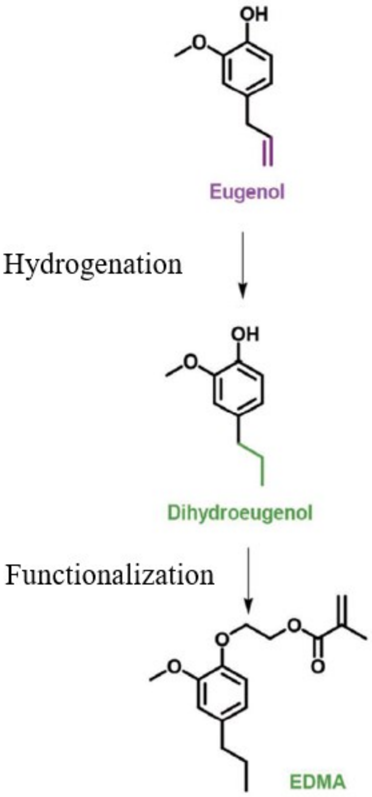

**Figure 2.1:** Chemical structures of eugenol, dihydroeugenol and ethoxy dihydroeugenyl methacrylate (EDMA). Adapted from *[53]*

In the second part of the work a copolymer of EDMA with coumarin, obtained with the reaction scheme in **Figure 2.2**, has been used as polymer matrix. More precisely, a copolymer with 1% of coumarin has been adopted, hereinafter referred to as EDMA-C1. EDMA-C1 was provided with 16,5% of TSC.

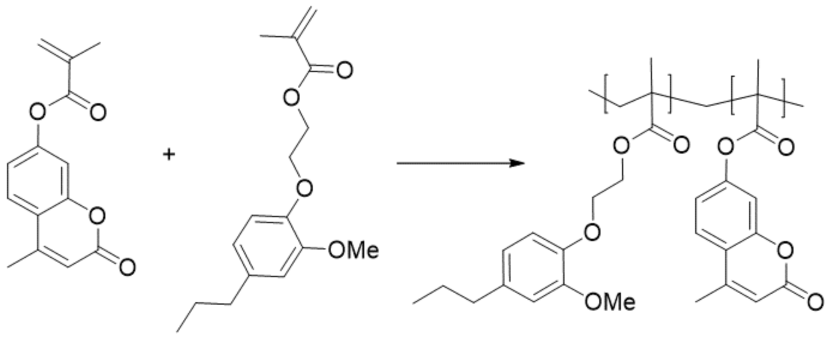

Figure 2.2: Reaction scheme for copolymerization of EDMA with coumarin

Both latexes were kindly provided by Dr.ssa Samantha Molina-Gutiérrez who synthesized them during her PhD at Montpellier University under the supervision of Dr. P. Lacroix-Desmazes [54].

## 2.2 Preparation of nanocomposites

As the first step of nanocomposite preparation, the commercial MFC paste is diluted in demineralized water to a concentration of 1%, 0,75%, 0,5% or 0,25% on weight basis. Homogenizer T 10 ULTRA-TURRAX® has been used to make MFC dispersion homogeneous. After obtaining the desired concentration, MFC suspension is added to latex. Once fixed the composition of the nanocomposite, the quantities of MFC and latex to use can be calculated depending on their concentrations.

Assuming $\rho_l = 1200$ [kg/m$^3$] as the density of latex and $\rho_{MFC} = 1500$ [kg/m$^3$] as the density of MFC, the density of nanocomposite film is calculated with Equation (2.1).

$$\rho_n = \frac{1}{\frac{w_l}{\rho_l}+\frac{w_{MFC}}{\rho_{MFC}}} \tag{2.1}$$

Where $w_l$ and $w_{MFC}$ are, respectively, the weight fractions of latex and MFC in the nanocomposite. Considering a nanocellulose content of 30% wt, $\rho_n = 1277$ [kg/m$^3$]. Once density of nanocomposite has been assessed, the total mass of the film can be calculated with Equation (2.2):

$$m_{tot} = \rho_n \cdot \frac{d^2}{4}\pi \cdot L \tag{2.2}$$

Where $d$ is the diameter of the Petri dish and $L$ is the desired thickness of the film. Once total mass of film has been evaluated, knowing the weight fractions of the components of the nanocomposite it is possible to calculate the amount of latex and MFC to be used.

Dispersion of MFC in the latex is obtained using a magnetic stirrer for 10 minutes at 1000 rpm. Solution is then submitted to vacuum to remove air bubbles originated by agitation. After degassing, the film-forming solution is cast on Petri dish of 80 [mm] of diameter and allowed to dry overnight under the fume hood. **Table 2.1** shows the amounts of latex and MFC dispersions used to produce the composites of the EDMA.

A similar procedure has been adopted for the preparation of the composites of EDMA-C1. In order to avoid excessive formation of air bubbles during agitation, dispersion of fillers is obtained by adding MFC suspension drop by drop into the latex while mixing with the magnetic stirrer at 700 rpm. Once all the necessary amount of MFC has been inserted, the solution is left on the magnetic stirrer for 10 minutes at 700 rpm. Degassing and solution-casting follow and the composite is left to dry under the hood. **Table 2.2** reports the quantities of components used to prepare the composites of the EDMA-C1.

The names of the composites contain the abbreviation of the polymer matrix (EDMA or EDMA-C1), the abbreviation of the cellulosic filler and its weight percentage (EV30 or EV5) and the concentration of the MFC suspension used in the preparation.

**Table 2.1:** Quantities of components used in the preparation of the nanocomposites of EDMA

| Nanocomposite | Components | Theoretical weight [g] | Actual weight [g] |
|---|---|---|---|
| EDMA-EV30-1 | EDMA-15TSC | 1,74 | 1,74 |
| | MFC-1% | 11,17 | 11,19 |
| EDMA-EV30-0,75 | EDMA-15TSC | 1,04 | 1,04 |
| | MFC-0,75% | 8,98 | 8,98 |
| EDMA-EV30-0,50 | EDMA-15TSC | 1,74 | 1,74 |
| | MFC-0,50% | 22,33 | 22,34 |
| EDMA-EV30-0,25 | EDMA-15TSC | 0,85 | 0,86 |
| | MFC-0,25% | 21,96 | 21,96 |
| EDMA-EV5-1 | EDMA-15TSC | 3,08 | 3,00 |
| | MFC-1% | 2,44 | 2,46 |

**Table 2.2:** Quantities of components used in the preparation of the nanocomposites of EDMA-C1

| Nanocomposite | Components | Theoretical weight [g] | Actual weight [g] |
|---|---|---|---|
| EDMA-C1-EV5-1 | EDMA-C1-16,5TSC | 3,51 | 3,54 |
| | MFC-1% | 3,04 | 3,04 |
| EDMA-C1-EV5-0,75 | EDMA-C1-16,5TSC | 3,51 | 3,51 |
| | MFC-0,75% | 4,06 | 4,02 |
| EDMA-C1-EV30-1 | EDMA-C1-16,5TSC | 1,58 | 1,59 |
| | MFC-1% | 11,16 | 11,09 |
| EDMA-C1-EV30-0,75 | EDMA-C1-16,5TSC | 1,36 | 1,38 |
| | MFC-0,75% | 12,83 | 12,81 |

Composites obtained using a suspension with 0,75% MFC have been chosen for undergoing permeability and surface energy characterization as they appeared the most homogenous of the prepared films. As regards the EDMA composite with 5% of MFC, the only sample produced was selected. All the chosen composites are reported in **Table 2.3**.

**Table 2.3:** Composites chosen for permeability and surface energy characterization

| Nanocomposite |
|---|
| EDMA-EV5-1 |
| EDMA-EV30-0,75 |
| EDMA-C1-EV5-0,75 |
| EDMA-C1-EV30-0,75 |

*Hot pressing*

To remove wrinkles from samples, and decrease porosity, the films reported in **Table 2.3** were hot pressed before any further characterization. To do so, the samples were inserted between two silicon-coated slides and subjected to a pressure of 76 [mbar] at 85 [°C] for 1,5 hours.

*UV curing*

Due to photodimerization of coumarin, whose general scheme is reported in **Figure 2.3**, the composites obtained with EDMA-C1 can be subjected to cross-linking under UV curing. To stimulate this process, EDMA-C1 composite films were subjected to 20 [mW/cm$^2$] for 20 minutes.

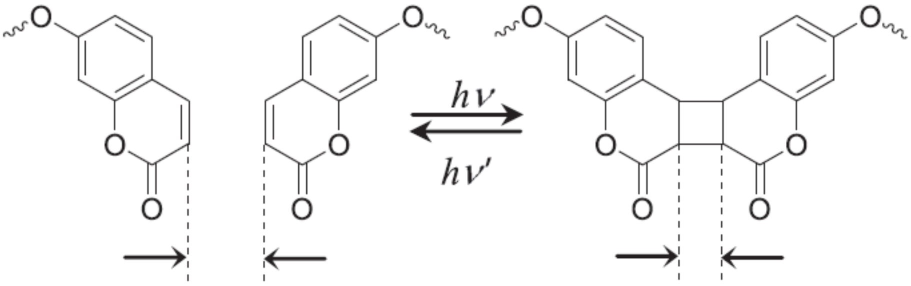

**Figure 2.3:** Photodimerization of coumarin derivatives. With permission from *[55]*

## 2.3 Characterization of the films

The morphology of nanocomposite has been analyzed using an optical microscope. Images were examined to evaluate the dispersion of MFC in the latex matrix.

The surface energy of nanocomposites was evaluated using Owens-Wendt method, which is based on the measurement of the static contact angle of the film samples with two different fluids (see Appendix II: Owens-Wendt method for the estimation of surface energy). In this work, water and hexadecane have been used. The contact angles have been measured with FTA1000 C Drop Shape Instrument at room temperature. Images were analyzed with FTA 32 software using the sessile drop technique.

## *2.4 Oxygen permeability test*

Oxygen permeability tests were conducted using Multi Perm: Oxygen & Water Vapor Permeability Analyser (MULTI 01/02/O2/H2O, ExtraSolution S.r.l.). This apparatus exploits the differential mode for the measurement of the Oxygen Transmission Rate OTR of a film sample. Films were examined under these conditions: T = 23 °C and RH = 0%. Samples were inserted in a surface reducer with an area of 2,01 $cm^2$ while film thickness was measured using a microcalibre, averaging out of 6 measurements per sample.

*Estimation of the diffusion coefficient*

Time-lag method, as described in chapter 1.3.3 Permeability tests, has been used for the estimation of the diffusion coefficient of oxygen in the composite polymer. More precisely, statistical moment method has been used to evaluate the moment $\mu_1$ which is equal to the time-lag $\tau_L$. $\mu_1$ was calculated using trapezoidal rule for the numerical integration of the experimental data.

The half-time point method has been used to have a second comparison value of the diffusion coefficient (see chapter 1.3.3 Permeability tests). The ascending section of the experimental curve was interpolated through a straight line and the half-time point was evaluated by requiring the fitting line to pass for half of the asymptotic value of OTR.

# 3. Results and discussion

## *3.1 Composite films*

Because of the short time available to access the laboratories and considering that composite production takes at least 24 hours, only few films could be produced. The first composites that were prepared were those with EDMA and 30% of MFC. Given the small amount of latex that was provided, only one sample of EDMA composite with 5% of cellulosic fillers has been prepared after the production of those with higher MFC content.

Four different concentrations of the MFC suspension have been tested to assess which was the optimal one to obtain homogeneous EDMA composite films. Suspension with 1% or 0,75% of MFC appeared more viscous than those with lower concentrations. A high viscosity could compromise both the dispersion of cellulosic fillers in latex and the degassing phase. On the other hand, the use of a less concentrated suspension implies having more water to be removed during drying under the hood.

By a visual observation of the films, EDMA-EV30-1 and EDMA-EV30-0,75 seemed to be the most homogeneous, although the first one had some air bubbles in few points of the film. As a result of these considerations, 1% and 0,75% MFC suspensions have been used to prepare the EDMA-C1 composites.

Both EDMA and EDMA-C1 composites appeared as almost transparent films. As an example, **Errore. L'origine riferimento non è stata trovata.** shows a composite film of EDMA-C1 with 5% of MFC, EDMA-C1-EV5-0,75. This film has some regions where the nanocellulose has not been adequately included. Probably, in the preparation phase agitation was not sufficient to ensure a good dispersion of MFC in the latex. A mild agitation was however preferred to avoid the formation of air bubbles that would have caused porosity within the films.

**Figure 3.1:** EDMA-C1-EV5-0,75 film

The appearance of haze that can be observed in the left pic of **Figure 3.1** could be due to light scattering. Indeed, light that is scattered on passing through a film can give an opaque appearance to the material. This phenomenon could be caused by the heterogeneity of the composite surface and by the roughness given by microfibrils.

The observation under optical microscope confirmed the absence of MFC in some parts of EDMA-C1-EV5-0,75 film, as shown in **Figure 3.2a.** Apart from these few spots, in general the microscope images exhibited a good dispersion of the MFC in the rest of the composite. **Figure 3.2b** shows how cellulose microfibrils have created a disordered s network structure within the polymer.

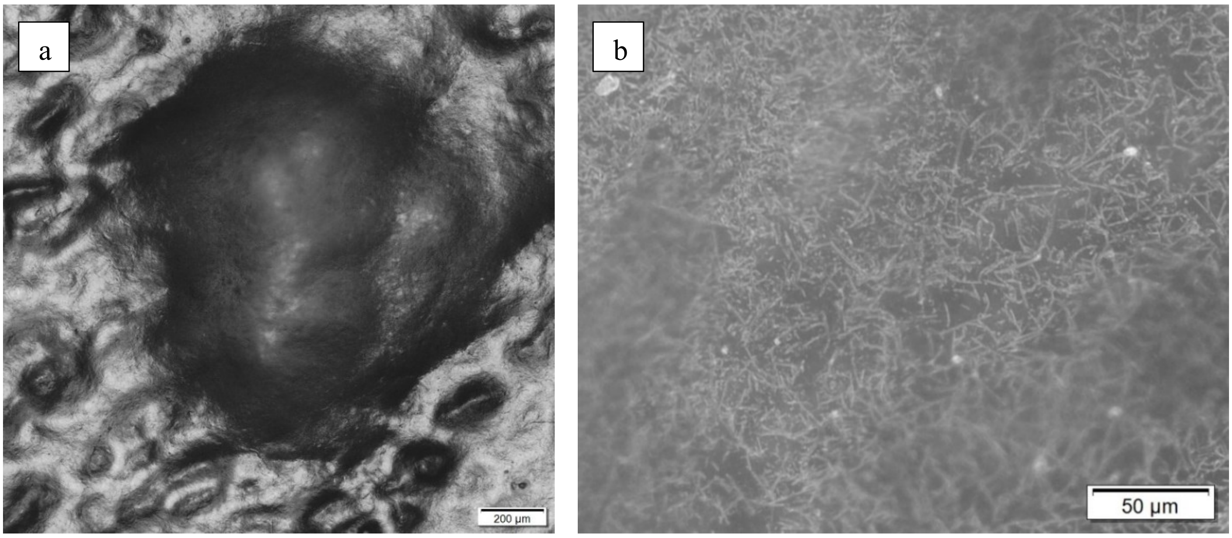

**Figure 3.2:** Images of EDMA-C1-EV5-0,75 film taken by optical microscope

The network of the microfibrillated cellulose shown in **Figure 3.2b** was also observed in the other composite films, as reported in **Figure 3.3**. These images show that cellulose nanofibers have created an exfoliated structure with many entanglements inside the latex. This morphology confirm that the introduction of fillers causes an increase of the tortuosity within the polymer matrix, which was the main purpose of the MFC insertion.

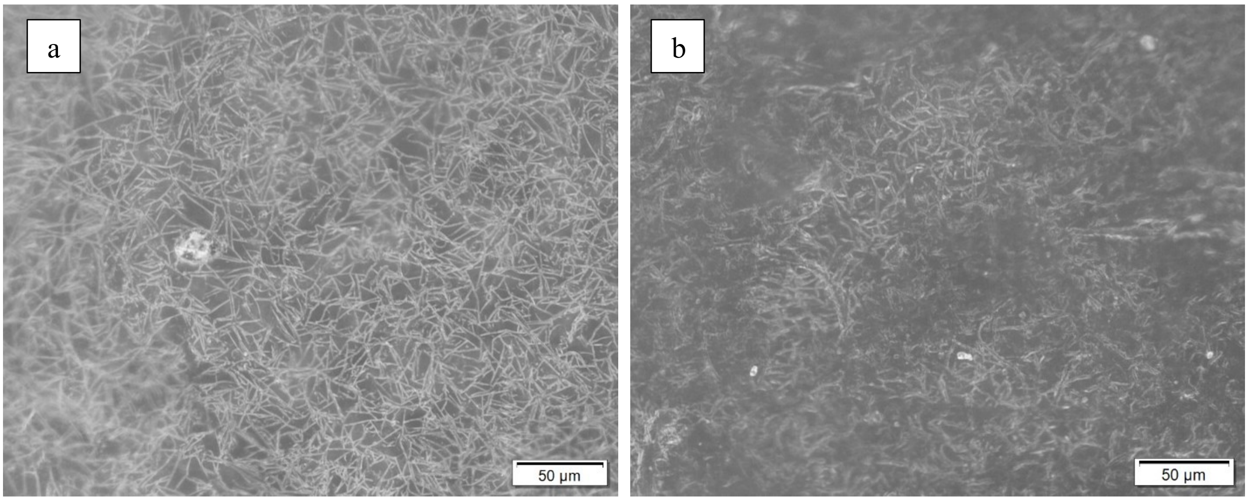

**Figure 3.3:** Microscope observations of MFC network within two polymer composites: a) EDMA-EV5-1 and b) EDMA-C1-EV30-0,75

Unlike EDMA-C1-EV5-0,75, the EDMA-C1 composite with 5% of microfibrillated cellulose obtained using a suspension with 1% MFC (EDMA-C1-EV5-1) exhibited some defects. First of all, after the drying process under the hood, the film was broken. Observations under optical microscope confirmed also the presence of microscopic holes, as shown **Errore. L'origine riferimento non è stata trovata.a**. In addition, **Figure 3.4b** shows some points where MFC is not well dispersed in the latex matrix. Due to these defects and the poor inclusion of nanocellulosic fillers, EDMA-C1-EV5-1 film was not used for permeability tests.

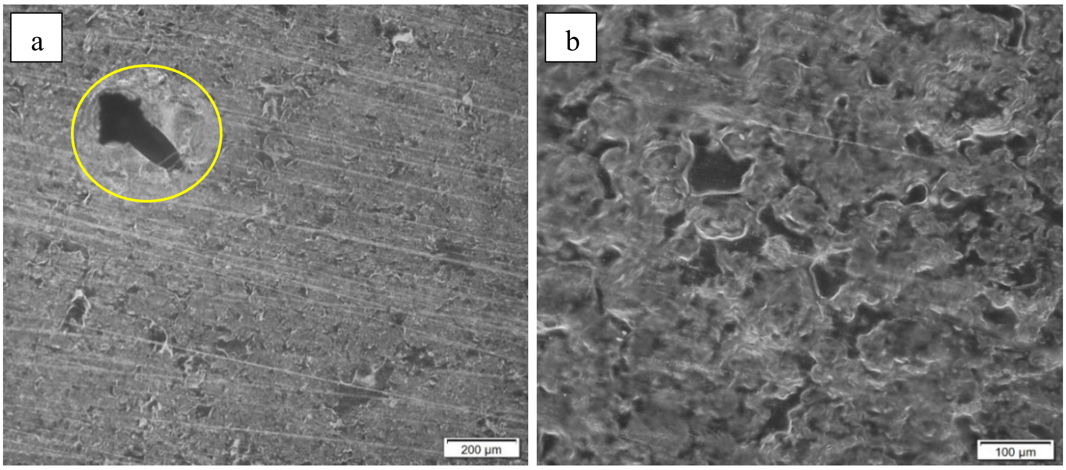

**Figure 3.4:** Images of EDMA-C1-EV5-1 film taken by optical microscope

*Hot-pressing*

After hot-pressing, all the films appeared more flattened and without wrinkles. Thanks to this procedure, it has been possible to better characterizes the composites films. Indeed, flatness of samples is fundamental both to analyze the images of the liquid drops for contact angles estimation and to have a good adhesion of the films on the surface reducer used for permeability test.

Microscope observations of films were repeated after the hot-pressing to evaluate possible changes in the morphology of composites. **Figure 3.5** shows that composites with 5% of cellulosic fillers preserved the network of nanofibers.

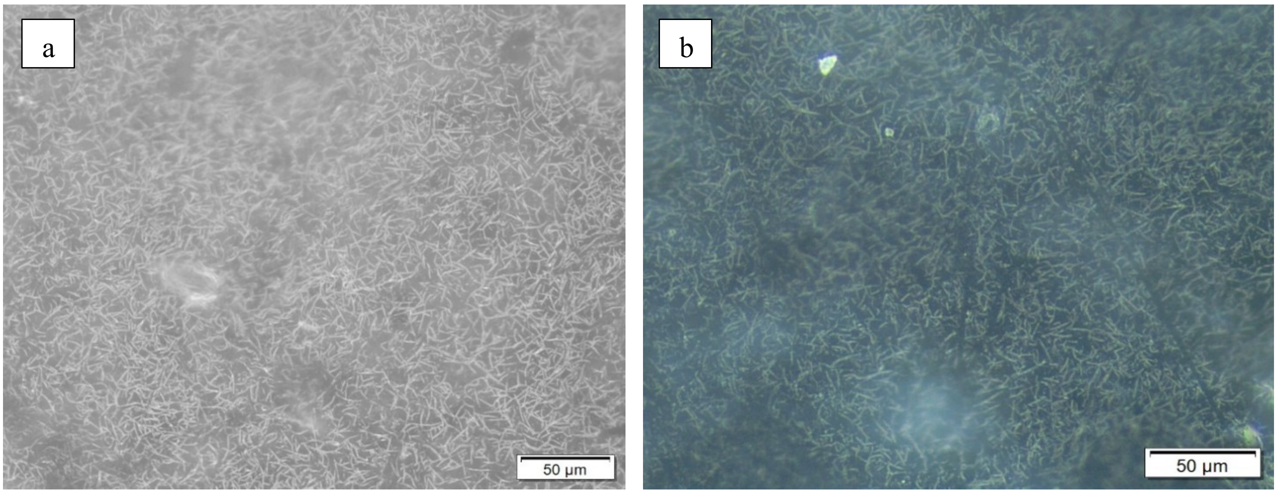

**Figure 3.5:** Microscope observations of composite films after hot-pressing: a) EDMA-EV5-1 and b) EDMA-C1-EV5-0,75

On the other hand, composites with 30% of MFC exhibited the formation of some cellulose agglomerates, as can be observed in **Figure 3.6**. Nevertheless, the desired increase in tortuosity is achieved.

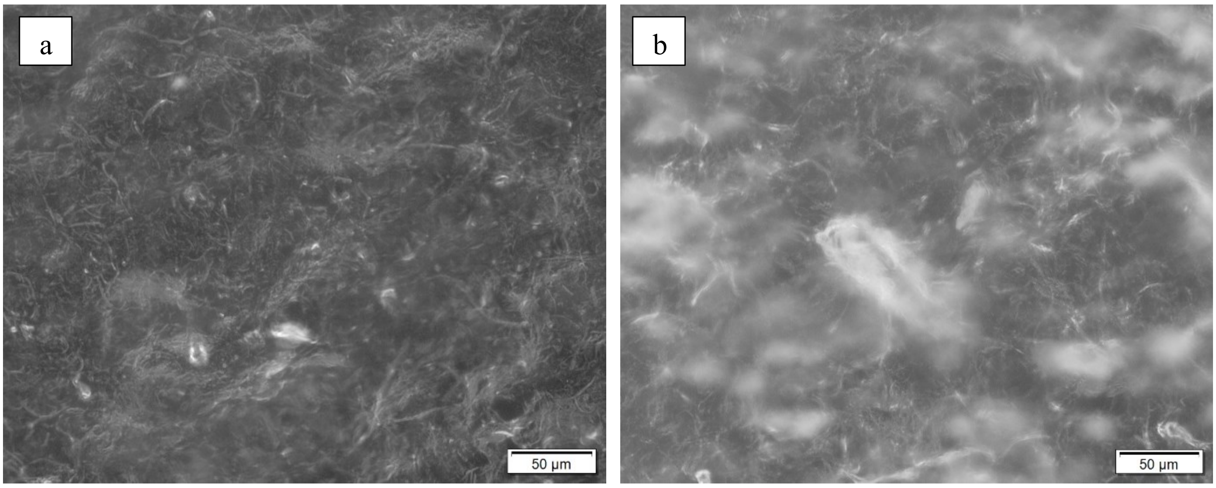

**Figure 3.6:** Microscope observations of composite films after hot-pressing: a) EDMA-EV30-0,75 and b) EDMA-C1-EV30-0,75

*UV curing*

Cross-linking was conducted directly on EDMA-C1 composite samples inserted into the surface reducer, after having performed the permeability test on the uncrosslinked film. **Figure 3.7** shows EDMA-C1-EV5-0,75 sample after the UV curing procedure.

**Figure 3.7:** EDMA-C1-EV5-0,75 sample after exposure to 20 [mW/cm$^2$] for 20 minutes

The sample reported in **Figure 3.7** has become yellow after the cross-linking process. Instead, EDMA-C1EV30-0,75 film subjected to UV curing remained white. Probably the higher cellulose content prevented a visible change in color.

## *3.2 Contact angles and surface energy*

Surface energy is an important parameter to assess in a polymeric material as its wettability properties depend on its value. With the prospect of a packaging application, it is important to know the adhesion and repellency properties of a material. For example, the material must ensure the adhesion of a label and therefore its surface must be wettable with an adhesive. Moreover, oil and water repellency can affect the appearance of the packaging. Both adhesion and repellency properties of a material depend on its surface energy.

**Table 3.1** shows the measurements of the contact angles with water and hexadecane of the composites whose permeability to oxygen has been investigated. Measurements were made after the hot-pressing process in order to avoid wrinkles that would have compromised the analysis of the images of the drops. For comparison, both EDMA and MFC films were characterized too. The reported values of the contact angles of the composite films were averaged over 5 measurements, while those of EDMA and MFC films derive from the mean of only 3 values since the samples had a small area.

The last columns of **Table 3.1** reports the values of the surface energy estimated with the Owens-Wendt method, reported in Appendix II: Owens-Wendt method for the estimation of surface energy. Since some samples have been characterized also after being immersed in distilled water, **Table 3.1** reports also the measurements made after the bath.

**Table 3.1:** Contact angles with water and hexadecane and surface energy of EDMA, MFC and composites films. Measurements before and after the bath are reported

| **Material** | **Contact Angle DI Water [°]** | | **Contact Angle Hexadecane [°]** | | **Surface energy [mN/m]** | |
|---|---|---|---|---|---|---|
| MFC | 59 ± 6 | | 36 ± 5 | | 44 | |
| | **Before** | **After** | **Before** | **After** | **Before** | **After** |
| EDMA | 31 ± 4 | 65 ± 2 | 36 ± 1 | 35 ± 6 | 63 | 40 |
| EDMA-EV5-1 | 33 ± 16 | 60 ± 18 | 36 ± 2 | 30 ± 8 | 62 | 45 |
| EDMA-EV30-0,75 | 57 ± 6 | 70 ± 2 | 34 ± 4 | 20 ± 9 | 45 | 38 |
| EDMA-C1-EV5-0,75 | 24 ± 4 | 35 ± 6 | 36 ± 2 | 41 ± 1 | 67 | 61 |
| EDMA-C1-EV30-0,75 | 68 ± 7 | 71 ± 2 | 30 ± 2 | 12 ± 1 | 39 | 38 |

The EDMA film showed a low contact angle with water, 31 [°], while the polymer obtained from the same eugenol-derived methacrylate through photoinduced polymerization in bulk showed a contact angle with water of 92 [°] [56], thus much higher value than the one measured for the film obtained here from the latex. Inconsistency with the value found in literature may be due to the presence of a surfactant on the latex surface. Indeed, EDMA latex contains 4 wt% of sodium dodecyl sulfate (SDS) on polymer basis. It is plausible that SDS may be present on the surface of the film, thus acting as wetting agent.

To check this hypothesis, contact angle measurements were repeated after immersing the sample in distilled water. After this procedure, the contact angle with water of the EDMA film have increased to a value of 65 [°]. This could be due to the removal of the SDS from the surface of the film.

As regard the contact angles measured on the composites, their values are intermediate compared to those measured for the films obtained from EDMA latex and from MFC alone. As reported in **Table 3.1**, composites with 30% of MFC showed higher values of the water contact angle with respect to the composites with a lower cellulose content.

This difference could again be due to the presence of SDS in the latex. In the composites with a low MFC content, as seen for the EDMA latex, the surfactant at the surface of the films may decrease the value of the water contact angle. When the cellulose content increases, the hydrophilic part of SDS may be attracted by microfibrils, preventing the reorientation towards the water drop at the surface, thus reducing the effect on wettability.

Roughness is another factor that should be considered as it affects the surface energy of a solid. Composites with 30% of MFC could have a higher surface roughness than those with a lower content of microfibrils. This factor may have a role in determining the difference found in the water contact angles of the composites. To do a more in-depth analysis, a more accurate characterization of the films surface would be needed.

## *3.3 Oxygen Transmission Rate*

The Multi Perm permeometer was available for the measurements approximately for one week. All the films examined were subjected to the hot-pressing process described in the experimental section with the aim of reducing wrinkles in the samples.

EDMA-C1-EV30-1 was the first film to be examined: this first measurement was however interrupted because at the beginning of the test the instrument measured negative values of the Oxygen Transmission Rate, as reported in **Figure 3.8**.

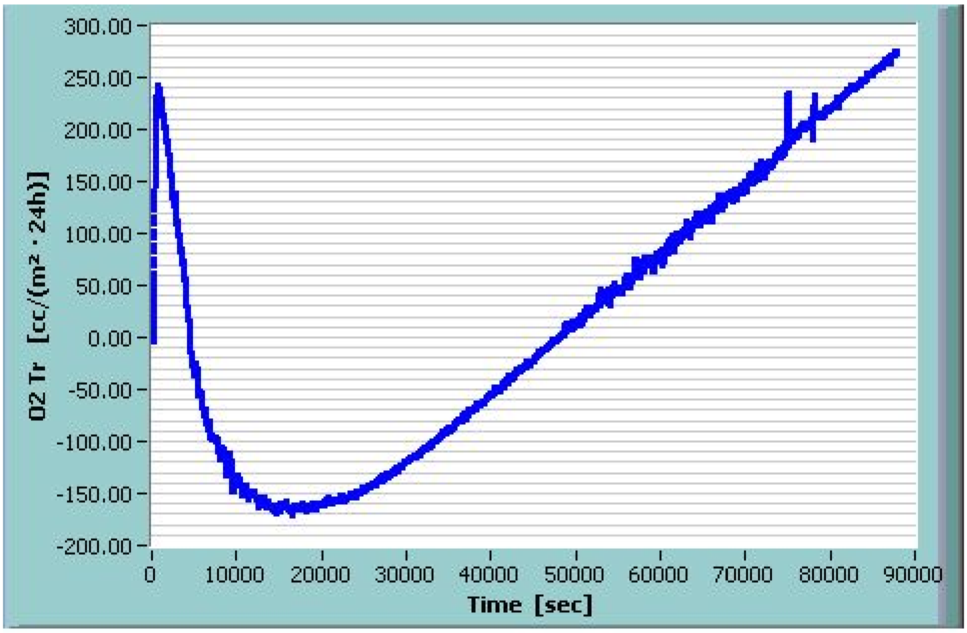

**Figure 3.8:** OTR experimental curve of EDMA-C1-EV30-1 film

This issue was attributed to a not sufficiently long time devoted to the conditioning of the experimental cell. Indeed, before starting the actual measurement of the OTR, Multi Perm permeometer performs a first conditioning cycle in which nitrogen is sent from both sides of the film to remove oxygen that entered the cell during the loading phase of the sample. The OTR value read at the end of the conditioning cycle is then used as baseline for the following measurement. In the case of EDMA-C1-EV30-1 test, conditioning lasted only 4 hours, while the OTR measurement had not yet reached a stable value after 24 hours.

To get more reliable results, subsequent tests were conducted by setting a minimum conditioning time of 20 hours, in order to have a good baseline value. Then, the OTR measurements actually reached a stable OTR value within less than two hours for all the films studied successively. However, due to the long conditioning time, it has been possible to carry out only a few tests.

**Figure 3.9** shows the experimental curves of the Oxygen Transmission Rate for EDMA composites, while **Figure 3.10** reports those of EDMA-C1 composites. All these experimental curves reflect the theoretical kinetic curve of the differential mode reported in **Figure 1.6b**.

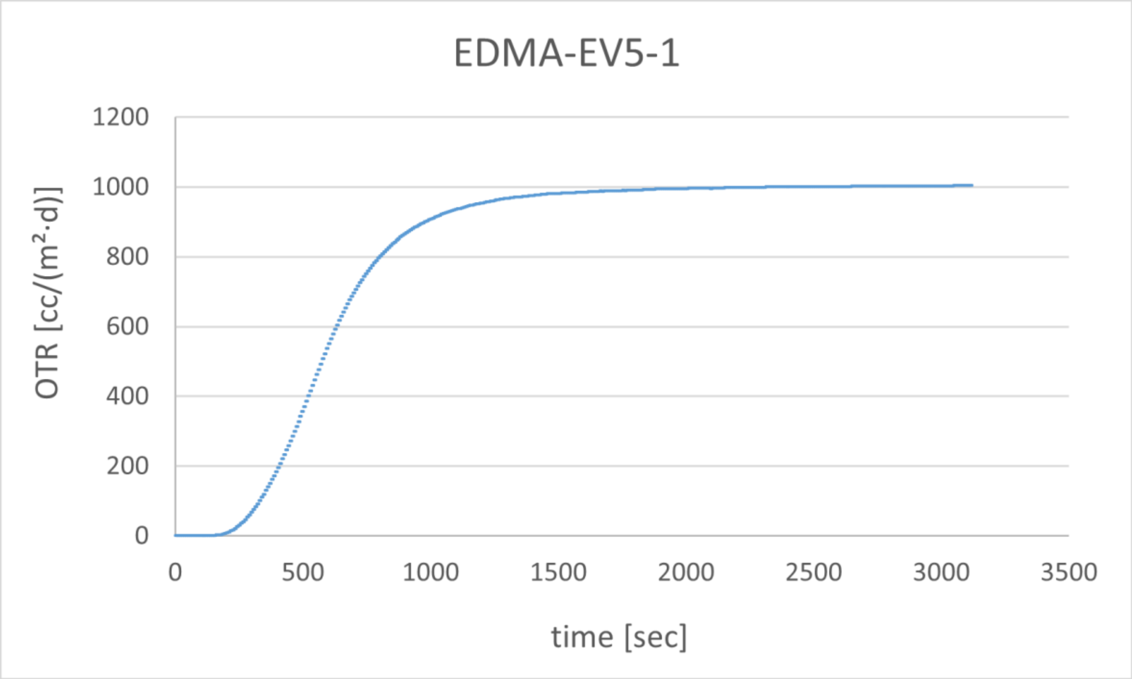

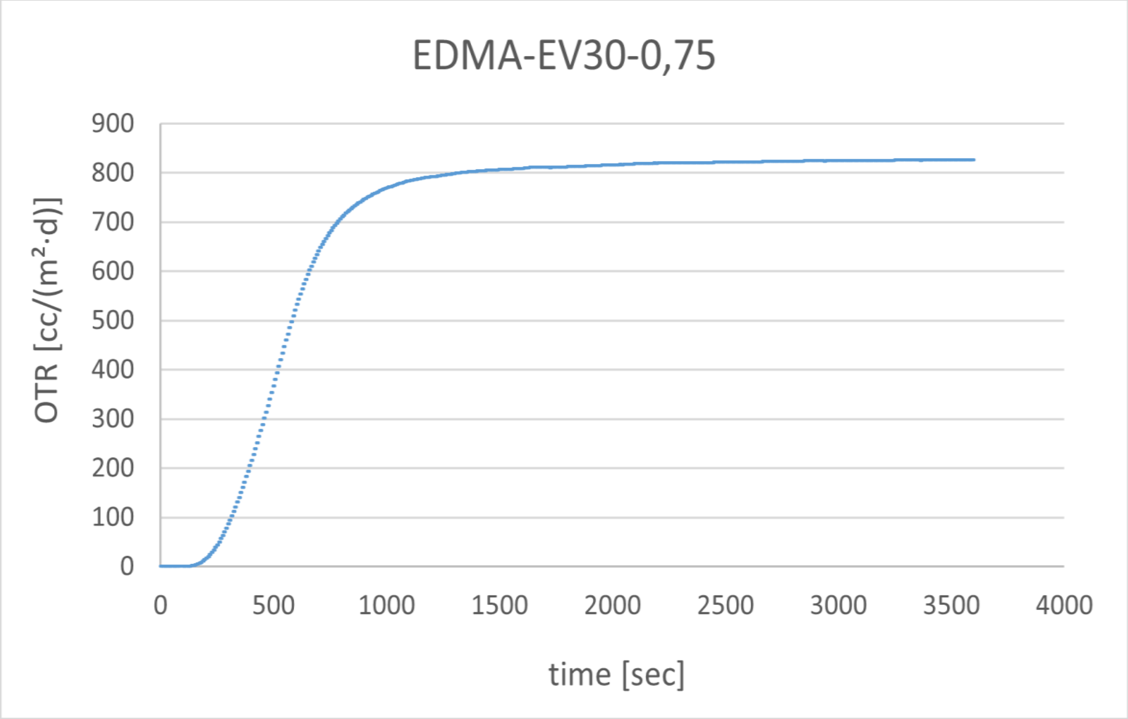

**Figure 3.9:** OTR experimental curves of EDMA composites

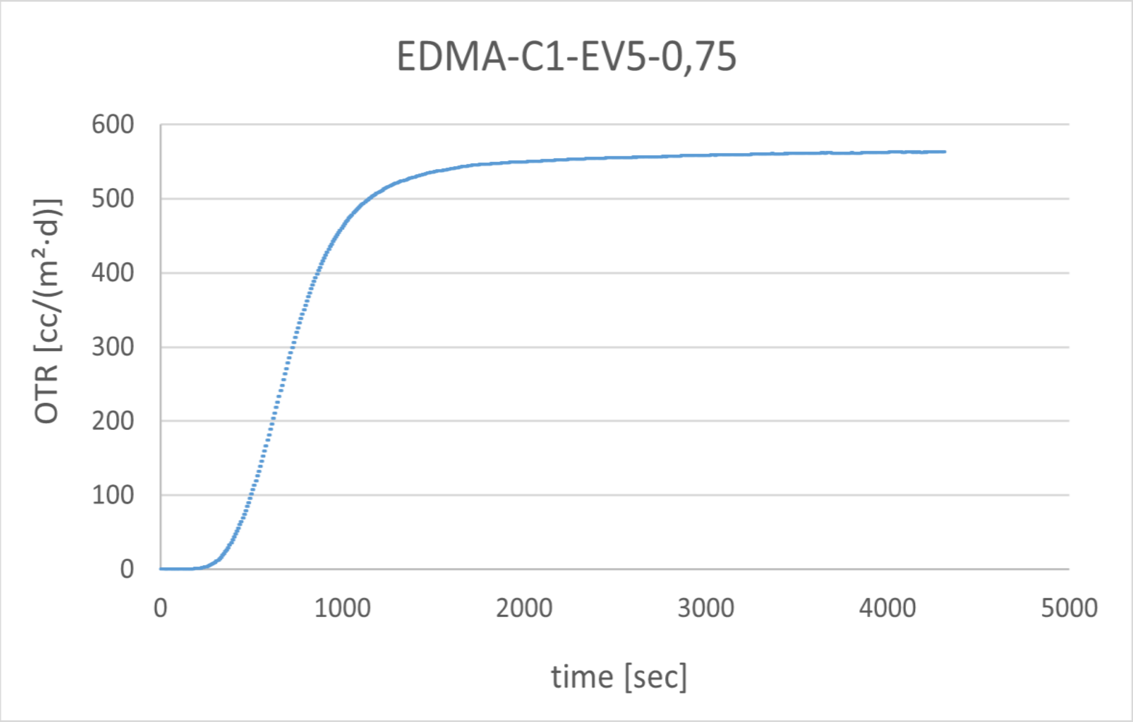

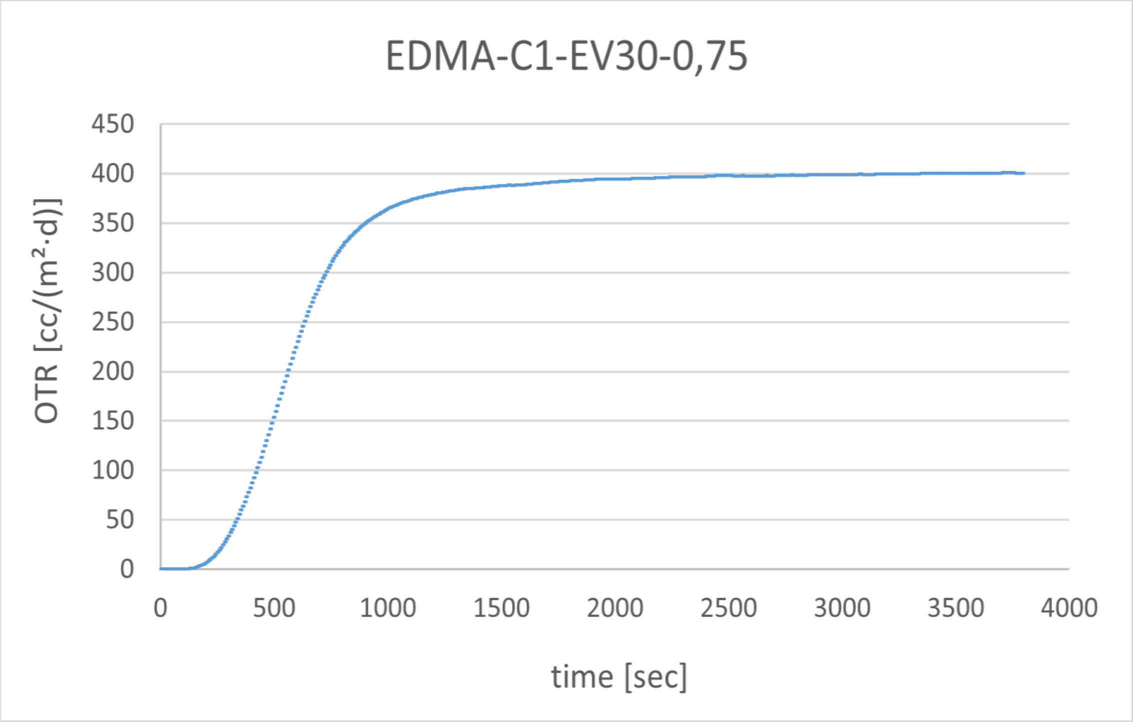

**Figure 3.10:** OTR experimental curves of EDMA-C1 composites

**Table 3.2** summarizes the test results in relation to the film thickness. To make a more objective comparison, OTR values have been normalized to a standard thickness of 25 [µm] and reported in **Table 3.2** as $OTR_{25}$.

**Table 3.2:** Effect of MFC content on the OTR of the composite films

| Nanocomposite | Thickness [µm] | OTR [cc/m$^2$ d] | OTR$_{25}$ [cc/m$^2$ d] |
|---|---|---|---|
| EDMA-EV5-1 | 143 ± 1 | 998 | 5713 |
| EDMA-EV30-0,75 | 55 ± 3 | 823 | 1816 |
| EDMA-C1-EV5-0,75 | 128 ± 5 | 561 | 2870 |
| EDMA-C1-EV30-0,75 | 52 ± 4 | 399 | 827 |

### 3.3.1 MFC content

Given the impossibility of obtaining a homogeneous film of EDMA alone with appropriate dimensions, to investigate the effect of MFC content on the barrier properties of the latexes, tests have been conducted on composite films with two different percentages of cellulosic fillers.

By comparing the normalized values of the Oxygen Transmission Rate OTR$_{25}$, the increase of the MFC content improved the barrier properties against oxygen for both the EDMA and the EDMA-C1 composites.

Specifically, increasing the MFC content from 5% to 30% caused a decrease of the OTR$_{25}$ of 71% in the EDMA-C1 composite films, while for EDMA composites there was a decrease of 68%.

These results confirm the improvement of barrier properties caused by the insertion of nanocellulose that was observed for other nanocomposites with cellulosic fillers reported in the literature.

*Diffusion coefficient*

Since the insertion of nanofillers has as its objective the increase of tortuosity of the diffusion path, the effect of the two different MFC contents can also be evaluated by calculating the diffusion coefficient.

**Table 3.3** shows the values of the diffusion coefficient estimated with the time-lag method and with the half-time point method, both described when differential mode of permeability tests was introduced (chapter 1.3.3 Permeability tests).

**Table 3.3:** Effect of MFC content on the diffusion coefficient of the composite films

| | Diffusion coefficient [cm$^2$/s] | |
|---|---|---|
| **Nanocomposite** | **Time-lag method** | **Half-time method** |
| EDMA-EV5-1 | $5{,}5 \cdot 10^{-8}$ | $5{,}0 \cdot 10^{-8}$ |
| EDMA-EV30-0,75 | $8{,}8 \cdot 10^{-9}$ | $8{,}1 \cdot 10^{-9}$ |
| EDMA-C1-EV5-0,75 | $3{,}5 \cdot 10^{-8}$ | $3{,}2 \cdot 10^{-8}$ |
| EDMA-C1-EV30-0,75 | $7{,}2 \cdot 10^{-9}$ | $6{,}7 \cdot 10^{-9}$ |

Comparing the values obtained with the two different methods, for the same sample the difference was always less than 10%. The half-time method is the easiest method to apply as it consists in reading a single time value from the experimental curve and substituting it in Equation (1.28). Its simplicity, however, makes it less precise than the time-lag method, which has been adapted to the differential mode through the calculation of the moment $\mu_1$ (see chapter 1.3.3 Permeability tests). Indeed, the moment method is based on the solution of the diffusion equation (1.17), using all the experimental data of the curve rather than a single point, and so it is more reliable [37].

Considering the values obtained through the time-lag method, the increase of the content of MFC from the 5% to the 30% on weight basis of the EDMA-C1 composites caused a decrease of the diffusion coefficient of the 80%. Regarding the effect for the EDMA composites, the diffusion coefficient decreased by 84% with the increase of MFC content. These results confirm the effect of increasing tortuosity caused by the introduction of nanofillers.

### 3.3.2 Coumarin effect

Another comparison that can be made is on the different polymer matrix at the same MFC content. **Table 3.2** shows that EDMA-C1 composites have much lower OTR values than those with EDMA as polymeric matrix.

In the composites with 5% of MFC content, the normalized value of the Oxygen Transmission Rate ($OTR_{25}$) decreased by 50% compared to the value obtained with the EDMA matrix when the EDMA-C1 copolymer matrix was used. Comparing composites with 30% of cellulosic fillers, the presence of coumarin caused a decrease of more than 54% of the $OTR_{25}$.

Making a similar comparison on diffusion coefficients reported in **Table 3.3**, the difference between the two latexes is less pronounced. In the composites with 5% of MFC content, the diffusion coefficient decreased by 36% from the EDMA matrix to that of EDMA-C1, while for the composites with 30% of cellulosic fillers, the presence of coumarin caused a decrease of only 18% of the diffusivity.

This weaker effect on the diffusion coefficient may mean that coumarin improves the barrier properties by acting also on solubility. Copolymerization with coumarin increases the number of polar groups in the polymer matrix and this could cause a decrease in the solubility of non-polar penetrants like oxygen. Moreover, the presence of polar groups also causes the formation of weak interactions within the copolymer chains and this may reduce the free volume of the polymer matrix and so decrease permeability.

### 3.3.3 UV curing

Cross-linking should cause a decrease in the free volume of the polymeric matrix through the formation of new chemical bonds which. Since permeation of gas occurs only in the free volume, this process should lead to a decrease in the permeability of the material.

To investigate the effect of the cross-linking process, UV curing was conducted directly on the EDMA-C1 composite samples previously used for permeability tests. **Table 3.4** shows the OTR values before and after this procedure.

**Table 3.4:** Effect of cross-linking on the OTR of the EDMA-C1 composite films

| | OTR [cc/m$^2$ d] | |
|---|---|---|
| **Nanocomposite** | **Before** | **After** |
| EDMA-C1-EV5-0,75 | 561 | 533 |
| EDMA-C1-EV30-0,75 | 399 | 300 |

Considering EDMA-C1-EV5-0,75, OTR only decreased by 5%. Instead, the EDMA-C1 composite with 30% of MFC content showed a slight improvement in its barrier properties: indeed, after the UV-curing, its OTR value decreased by about 25%.

Probably, the low effect of cross-linking on OTR is due to the low percentage of coumarin used in the copolymerization with EDMA. Since it is the photodimerization of coumarin that causes the formation of new chemical bonds, perhaps using a higher percentage of coumarin could cause a more noticeable improvement in the barrier properties after cross-linking.

### 3.3.4 Comparison with traditional plastics

To assess whether the material developed in this study is capable of competing with petroleum-based polymers, the oxygen permeability data of the polymer composites are compared with those of traditional plastics.

**Table 3.5** shows the Oxygen Transmission Rate values of some plastic films of 25 [μm] thickness evaluated at T = 23 [°C] and RH = 0% [34]. The experimental OTR values, normalized to the same thickness, of EDMA and EDMA-C1 composites are reported at the bottom of the table with the purpose of comparison.

**Table 3.5:** Comparison of EDMA and EDMA-C1 composites with petroleum-based polymers in terms of $OTR_{25}$ values. Data of traditional plastics are reported from *[34]*

| **Polymer** | **$OTR_{25}$ [cc/(m$^2$ d)]** |
|---|---|
| Low density polyethylene | 7400 |
| High density polyethylene | 1600 |
| Polypropylene (oriented) | 1550 |
| Polyethylene terephthalate | 55 |
| Polyamide (nylon) 6,6 | 35 |
| EDMA-EV5-1 | 5713 |
| EDMA-EV30-0,75 | 1816 |
| EDMA-C1-EV5-0,75 | 2870 |
| EDMA-C1-EV30-0,75 | 827 |
| EDMA-C1-EV5-0,75-UV | 2729 |
| EDMA-C1-EV30-0,75-UV | 623 |

Among the composites examined, only EDMA-C1-EV30-0,75 has competitive values of the Oxygen Transmission Rate, both before and after cross-linking. Indeed, the composite has OTR values much lower compared to those of LDPE, HDPE or PP. However, when compared with materials such as PET or nylon, the composite shows higher values of the Oxygen Transmission Rate. In summary, the EDMA-C1 composite with 30% of MFC has medium barrier properties towards oxygen.

To understand the actual validity of a material in a packaging application, besides the barrier properties to oxygen, permeability towards other gases such as CO2 or water should be studied, as well as the influence of temperature and relative humidity on such properties. Unfortunately, due to the limited time that it was possible to devote to the experimental investigation, it was not possible to deepen the study of barrier properties.

However, the main difference that must be kept in mind in comparison with traditional plastics is that, unlike the latter, the composite materials studied in this work meets several sustainability criteria.

The polymer matrix consists of a biobased latex obtained from a derivative of eugenol, more precisely a methacrylate of dihydroeugenol. Eugenol is a natural phenol that can be extracted from several plant resources. For example, eugenol may be obtained by depolymerization of lignin, one of the main components of lignocellulosic biomass with cellulose and hemicellulose. Considering that lignin is the non-edible portion of the plant, its use in producing biobased monomers such as eugenol would not compete with food supply [57].

In addition to the renewability of the source, the production process of the latex is sustainable too. After the insertion of the methacrylate group and the obtaining of EDMA monomer through the procedure described by Molina-Gutiérrez et al. [53], aqueous emulsion polymerization can be performed to obtain a stable latex of poly(ethoxy dihydroeugenyl methacrylate). This process has been studied in another work of Molina-Gutiérrez et al. [54].

Since it does not require the use of harmful solvents, aqueous emulsion polymerization can be considered as an environmentally friendly polymerization method. Moreover, also the cross-linking thorough UV-curing used on EDMA-C1 composites is a sustainable process.

Regarding the nanofillers, as discussed in the introduction, several renewable sources are available for nanocellulose production. In addition to renewability, another beneficial feature of cellulose is its biodegradability. Both these characteristics are highly sought-after in the development of innovative materials for packaging application. Indeed, the use of recyclable packaging from renewable sources could improve the waste disposal and reduce the dependence on petroleum-based polymers.

# 4. Conclusions

The objective of this thesis was the study of the properties to the gas transport of polymers reinforced with cellulosic fillers.

The study of the data collected in the literature showed that the insertion of nanocellulose causes an improvement in the barrier properties of a polymer matrix. This effect can be explained considering that fillers induce a greater tortuosity in the diffusion path of a permeant gas.

To have a confirmation of the analysis made on the literature data, the second part of the work was to study the permeability towards water vapor and oxygen of a biobased latex reinforced with microfibrillated cellulose. Unfortunately, due to lack of time, composites have been characterized only as regards their barrier properties towards oxygen, considering only low relative humidity conditions.

The few data collected confirmed the hypotheses found in the literature: the insertion of cellulosic fillers enhances the barrier properties of a polymer matrix. Indeed, increasing the MFC content from 5% to 30% caused a decrease of almost the 70% in the Oxygen Transmission Rate of the examined composites. Probably a further increase in the cellulose content could give a further improvement.

This improvement in barrier properties was confirmed by the lowering of gas diffusion coefficient in the latex composites. Both EDMA and EDMA-C1 composites showed a reduction of 80% in the diffusion coefficient after the increase of cellulosic fillers. This evident decrease confirms that the main effect of the insertion of fillers is increasing the tortuosity within the polymer matrix.

Another strategy that has been attempted to improve the barrier properties was the cross-linking of the composite material obtained using a copolymer of EDMA with coumarin as matrix. Cross-linking should improve the barrier properties of a polymeric material by reducing its free volume, where permeation of gases takes place. This effect, however, did not occur so clearly as the effect of cellulosic fillers did. In the best case, after cross-linking OTR value decreased by only 25%, while in the other case this reduction was not even by 5%. It would be interesting to assess whether using a copolymer with a higher percentage of coumarin there would be a more significant improvement in the barrier properties after cross-linking.

In comparison with traditional plastics, only EDMA-C1-EV30-0,75 showed competitive values of the Oxygen Transmission Rate. However, in order to establish its validity as packaging material, further investigations should be carried out.

With this perspective, barrier properties towards other gases such as water vapor and carbon dioxide should be investigated. Moreover, it would be interesting also to evaluate the effect of relative humidity and temperature on permeability. Other compositions of the composites could be analyzed too, either as regards the MFC content or as regards the coumarin percentage in the EDMA copolymer.

# References

[1] Plastics Europe, "Plastics - the Facts 2019," [Online]. Available: https://www.plasticseurope.org/it/resources/publications/1804-plastics-facts-2019. [Accessed 15 03 2021].

[2] F. Luzi, L. Torre, J. M. Kenny, D. Puglia, "Bio- and Fossil-Based Polymeric Blends and Nanocomposites for Packaging: Structure–Property Relationship," *Materials,* vol. 12, no. 3, p. 471, 2019.

[3] European Commission, "A European Strategy for Plastics in a Circular Economy," 16 01 2018. [Online]. Available: https://eur-lex.europa.eu/legal-content/IT/TXT/?uri=COM%3A2018%3A28%3AFIN. [Accessed 15 03 2021].

[4] European Parliament, "Directive (EU) 2018/852," 30 05 2018. [Online]. Available: https://eur-lex.europa.eu/legal-content/EN/TXT/?uri=celex:32018L0852. [Accessed 15 03 2021].

[5] E. L. Sánchez-Safont, A. Aldureid, J. M. Lagarón, J. Gámez-Pérez, L. Cabedo, "Biocomposites of different lignocellulosic wastes for sustainable food packaging applications," *Composites Part B,* vol. 145, pp. 215-225, 2018.

[6] F. Li, E. Mascheroni, L. Piergiovanni, "The Potential of NanoCellulose in the Packaging Field: A Review," *Packaging Technology and Science,* vol. 28, no. 6, pp. 475-508, 2015.

[7] N. Lavoine, I. Desloges, A. Dufresne, J. Bras, "Microfibrillated cellulose – Its barrier properties and applications in cellulosic materials: A review," *Carbohydrate Polymers,* vol. 90, no. 2, p. 735– 764, 2012.

[8] Y. Habibi, L. A. Lucia, O. J. Rojas, "Cellulose Nanocrystals: Chemistry, Self-Assembly, and Applications," *Chemical Reviews,* vol. 110, no. 6, p. 3479–3500, 2010.

[9] U. Qasim, A. I. Osman, A. H. Al-Muhtaseb, C. Farrell, M. Al-Abri, M. Ali, D. N. Vo, F. Jamil, D. W. Rooney, "Renewable cellulosic nanocomposites for food packaging to avoid fossil fuel plastic pollution: a review," *Environmental Chemistry Letters,* vol. 19, pp. 613-641, 2021.

[10] A.N. Nakagaito, H. Yano, "The effect of morphological changes from pulp fiber towards nano-scale fibrillated cellulose on the mechanical properties of high-strength plant fiber based composites," *Applied Physics A –Materials Science & Processing,* vol. 78, p. 547–552, 2004.

[11] A. López-Rubio, J.M. Lagaron, M. Ankerfors, T. Lindström, D. Nordqvist, A. Mattozzi, M.S. Hedenqvist, "Enhanced fillm forming and film properties of amylopectin using micro-fibrillated cellulose," *Carbohydrate Polymers,* vol. 68, p. 718–727, 2007.

[12] A. Alemdar, M. Sain, "Isolation and characterization of nanofibers from agricultural residues – Wheat straw and soy hulls," *Bioresource Technology,* vol. 99, p. 1664–1671, 2008.

[13] S. Iwamoto, A.N. Nakagaito, H. Yano, "Nano-fibrillation of pulp fibers for the processing of transparent nanocomposites," *Applied Physics A,* vol. 89, p. 461–466, 2007.

[14] M. Paakko, M. Ankerfors, H. Kosonen, A. Nykanen, S. Ahola, M. Osterberg, J. Ruokolainen, J. Laine, P. T. Larsson, O. Ikkala, T. Lindstrom, "Enzymatic Hydrolysis Combined with Mechanical Shearing and High-Pressure Homogenization for Nanoscale Cellulose Fibrils and Strong Gels," *Biomacromolecules,* vol. 8, pp. 1934-1941, 2007.

[15] T. Taipale, M. Osterberg, A. Nykanen, J. Ruokolainen, J. Laine, "Effect of microfibrillated cellulose and fines on the drainage of kraft pulp suspension and paper strength," *Cellulose,* vol. 17, p. 1005–1020, 2010.

[16] A. Isogai, T. Saito, H. Fukuzumi, "TEMPO-oxidized cellulose nanofibers," *Nanoscale,* vol. 3, pp. 71-85, 2011.

[17] M. Henriksson, L. A. Berglund, P. Isaksson, T. Lindstrom, T. Nishino, "Cellulose Nanopaper Structures of High Toughness," *Biomacromolecules,* vol. 9, p. 1579–1585, 2008.

[18] I. Siró , D. Plackett, M. Hedenqvist, M. Ankerfors, T. Lindström, "Highly Transparent Films from Carboxymethylated Microfibrillated Cellulose: The Effect of Multiple Homogenization Steps on Key Properties," *Journal of Applied Polymer Science,* vol. 119, p. 2652–2660 , 2011.

[19] K. Syverud, P. Stenius, "Strength and barrier properties of MFC films," *Cellulose,* vol. 16, p. 75–85, 2009.

[20] M. Österberg, J. Vartiainen, J. Lucenius, U. Hippi, J. Seppälä, R. Serimaa, J. Laine, "A Fast Method to Produce Strong NFC Films as a Platform for Barrier and Functional Materials," *ACS Applied Materials & Interfaces,* vol. 5, p. 4640−4647, 2013.

[21] Y. C. Gorur, P. A. Larsson, L. Wågberg, "Self-Fibrillating Cellulose Fibers: Rapid In Situ Nanofibrillation to Prepare Strong, Transparent, and Gas Barrier Nanopapers," *Biomacromolecules,* vol. 21, pp. 1480-1488, 2020.

[22] C. Aulin, M. Gallstedt, T. Lindstrom, "Oxygen and oil barrier properties of microfibrillated cellulose films and coatings," *Cellulose,* vol. 17, p. 559–574, 2010.

[23] I. Siró, D. Plackett, "Microfibrillated cellulose and new nanocomposite materials: a review," *Cellulose,* vol. 17, pp. 459-494, 2010.

[24] R. A. Ilyas, S. M. Sapuan, M. R. Ishak, E. S. Zainudin, "Sugar palm nanocrystalline cellulose reinforced sugar palm starch composite: Degradation and water-barrier properties," *Materials Science and Engineering,* vol. 368, p. 012006, 2018.

[25] A. Lepetit, R. Drolet, B. Tolnai, R. Zerrouki, D. Montplaisir, "Effect of acetylation on the properties of microfibrillated cellulose-LDPE composites," *Journal of Applied Polumer Science,* vol. 134, p. 44933, 2017.

[26] G. Rodionova, M. Lenes, Ø. Eriksen, Ø. Gregersen, "Surface chemical modification of microfibrillated cellulose: improvement of barrier properties for packaging applications," *Cellulose,* vol. 18, p. 127–134, 2011.

[27] M. L. Hassan, J. Bras, E. A. Hassan, S. M. Fadel, A. Dufresne, "Polycaprolactone/Modified Bagasse Whisker Nanocomposites with Improved Moisture-Barrier and Biodegradability Properties," *Journal of Applied Polymer Science,* vol. 125, p. E10–E19, 2012.

[28] N. Ljungberg, C. Bonini, F. Bortolussi, C. Boisson, L. Heux, J.Y. Cavaillé, "New Nanocomposite Materials Reinforced with Cellulose Whiskers in Atactic Polypropylene: Effect of Surface and Dispersion Characteristics," *Biomacromolecules,* vol. 6, pp. 2732-2739, 2005.

[29] S. Phomrak, M. Phisalaphong, "Reinforcement of Natural Rubber with Bacterial Cellulose via a Latex Aqueous Microdispersion Process," *Journal of Nanomaterials,* vol. 2017, p. 9, 2017.

[30] S. K. Sharma, P. R. Sharma, S. Lin, H. Chen, K. Johnson, R. Wang, W. Borges, C. Zhan, B. S. Hsiao, "Reinforcement of Natural Rubber Latex Using Jute

Carboxycellulose Nanofibers Extracted Using Nitro-Oxidation Method," *Nanomaterials,* vol. 10, p. 706, 2020.

[31] R. Stephen, C. Ranganathaiah, S. Varghese, K. Joseph, S. Thomas, "Gas transport through nano and micro composites of natural rubber (NR) and their blends with carboxylated styrene butadiene rubber (XSBR) latex membranes," *Polymer,* vol. 47, pp. 858-870, 2006.

[32] Y. Guan, K. P. Meyers, S. K. Mendon, G. Hao, J. R. Douglas, S. Trigwell, S. I. Nazarenko, D. L. Patton, J. W. Rawlins, "Ecofriendly Fabrication of Modified Graphene Oxide Latex Nanocomposites with High Oxygen Barrier Performance," *Applied Materials & Interfaces,* vol. 8, p. 33210−33220, 2016.

[33] H. E. Lockhart, "A Paradigm for Packaging," *Packaging Technology and Science,* vol. 10, p. 237–252, 1997.

[34] G. L. Robertson, Food Packaging: Principles and Practice, 3rd ed., Boca Raton: Taylor & Francis Group, 2013, pp. 2-4, 98-122.

[35] G. Choudalakis, A.D. Gotsis, "Permeability of polymer/clay nanocomposites: A review," *European Polymer Journal,* vol. 45, pp. 967-984, 2009.

[36] I.N. Beckman, D.A. Syrtsova, M.G. Shalygin, P. Kandasamy, V.V. Teplyakov, "Transmembrane gas transfer: Mathematics of diffusion and experimental practice," *Journal of Membrane Science,* vol. 601, p. 117737, 2020.

[37] R.M. Felder, "Estimation of gas transport coefficients from differential permeation, integral permeation, and sorption rate data," *Journal of Membrane Science,* vol. 15, pp. 15-27, 1978.

[38] K. Prasad, M. Nikzad, I. Sbarski, "Permeability control in polymeric systems: a review," *Journal of Polymer Research,* vol. 25, p. 232, 2018.

[39] J.-W. Rhim, P.K. W. Ng, "Natural Biopolymer-Based Nanocomposite Films for Packaging Applications," *Critical Reviews in Food Science and Nutrition,* vol. 47, pp. 411-433, 2007.

[40] V. Kumar, R. Bollström, A. Yang, Q. Chen, G. Chen, P. Salminen, D. Bousfield, M. Toivakka, "Comparison of nano- and microfibrillated cellulose films," *Cellulose,* vol. 21, p. 3443–3456, 2014.

[41] A. H. Tayeb, M. Tajvidi, D. Bousfield, "Enhancing the Oxygen Barrier Properties of Nanocellulose at High Humidity: Numerical and Experimental Assessment," *Sustainable Chemistry,* vol. 1, pp. 198-208, 2020.

[42] J. Xia, Z. Zhang, W. Liu, V. C. F. Li, Y. Cao, W. Zhang, Y. Deng, "Highly transparent 100% cellulose nanofibril films with extremely high oxygen barriers in high relative humidity," *Cellulose,* vol. 25, p. 4057–4066, 2018.

[43] L. Wang, C. Chen, J. Wang, D. J. Gardner, M. Tajvidi, "Cellulose nanofibrils versus cellulose nanocrystals: Comparison of performance in flexible multilayer films for packaging applications," *Food Packaging and Shelf Life,* vol. 23, p. 100464, 2020.

[44] B. Bideau, J. Brasb, N. Adoui, E. Loranger, C. Daneault, "Polypyrrole/nanocellulose composite for food preservation: Barrier and antioxidant characterization," *Food Packaging and Shelf Life,* vol. 12, pp. 1-8, 2017.

[45] D. Plackett, H. Anturi, M. Hedenqvist, M. Ankerfors, M. Gällstedt, T. Lindström, I. Siro, "Physical Properties and Morphology of Films Prepared from Microfibrillated Cellulose and Microfibrillated Cellulose in Combination with Amylopectin," *Journal of Applied Polymer Science,* vol. 117, pp. 3601-3609, 2010.

[46] M. D. Sanchez-Garcia, J. M. Lagaron, "On the use of plant cellulose nanowhiskers to enhance the barrier properties of polylactic acid," *Cellulose,* vol. 17, pp. 987-1004, 2010.

[47] G. Rodionova, T. Saito, M. Lenes, Ø. Eriksen, Ø. Gregersen, H. Fukuzumi, A. Isogai, "Mechanical and oxygen barrier properties of films prepared from fibrillated dispersions of TEMPO-oxidized Norway spruce and Eucalyptus pulps," *Cellulose,* vol. 19, p. 705–711, 2012.

[48] S. Fujisawa, Y. Okita, H. Fukuzumi, T. Saito, A. Isogai, "Preparation and characterization of TEMPO-oxidized cellulose nanofibril films with free carboxyl groups," *Carbohydrate Polymers,* vol. 84, pp. 579-583, 2011.

[49] J. Kim, B. Choi, J. Jin, "Transparent, water-stable, cellulose nanofiber-based packaging film with a low oxygen permeability," *Carbohydrate Polymers,* vol. 249, p. 116823, 2020.

[50] M.D. Sanchez-Garcia, E. Gimenez, J.M. Lagaron, "Morphology and barrier properties of solvent cast composites of thermoplastic biopolymers and purified cellulose fibers," *Carbohydrate Polymers,* vol. 71, pp. 235-244, 2008.

[51] H. M.C. Azeredo, L. H. C. Mattoso, D. Wood, T. G. Williams, R. J. Avena-Bustillos, T. H. McHugh, "Nanocomposite Edible Films from Mango Puree Reinforced with Cellulose Nanofibers," *Journal of food science,* vol. 74, pp. N31-N35, 2009.

[52] H. M. C. Azeredo, L. H. C. Mattoso, R. J. Avena-Bustillos, G. C. Filho, M. L. Munford, D. Wood, T. H. McHugh, "Nanocellulose Reinforced Chitosan Composite Films as Affected by Nanofiller Loading and Plasticizer Content," *Journal of Food Science,* vol. 75, pp. N1-N7, 2010.

[53] S. Molina-Gutiérrez, A. Manseri, V. Ladmiral, R. Bongiovanni, S. Caillol, P. Lacroix-Desmazes, "Eugenol: A Promising Building Block for Synthesis of Radically Polymerizable Monomers," *Macromolecular Chemistry and Physics,* vol. 220, p. 1900179, 2019.

[54] S. Molina-Gutiérrez, V. Ladmiral, R. Bongiovanni, S. Caillol, P. Lacroix-Desmazes, "Emulsion Polymerization of Dihydroeugenol-, Eugenol-, and Isoeugenol-Derived Methacrylates," *Industrial & Engineering Chemistry Research,* vol. 58, pp. 21155-21164, 2019.

[55] E. Sato, S. Nagai, A. Matsumoto, "Reversible thickness control of polymer thin films containing photoreactive coumarin derivative units," *Progress in Organic Coatings,* vol. 76, pp. 1747-1751, 2013.

[56] S. Molina-Gutiérrez, S. Dalle Vacche, A. Vitale, V. Ladmiral, S. Caillol, R. Bongiovanni, P. Lacroix-Desmazes, "Photoinduced Polymerization of Eugenol-Derived Methacrylates," *Molecules,* vol. 25, p. 3444, 2020.

[57] S. Molina-Gutiérrez, V. Ladmiral, R. Bongiovanni, S. Caillol, P. Lacroix-Desmazes, "Radical polymerization of biobased monomers in aqueous dispersed media," *Green Chemistry,* vol. 21, pp. 36-53, 2019.

[58] M. Giacinti Baschetti, M. Minelli, "Test methods for the characterization of gas and vapor permeability in polymers for food packaging application: A review," *Polymer Testing,* vol. 89, p. 106606, 2020.

[59] E. Chibowski, "Some problems of characterization of a solid surface via the surface free energy changes," *Adsorption Science & Technology,* vol. 35, pp. 647-659, 2017.

[60] C. Goussé, H. Chanzy, M.L. Cerrada, E. Fleury, "Surface silylation of cellulose microfibrils: preparation and rheological properties," *Polymer,* vol. 45, p. 1569–1575, 2004.

# List of figures

# List of tables

# Appendix I: Permeability coefficient units and conversion factors

Consideration of Equation (1.11) shows the dimension of the *permeability coefficient $K_P$* to be:

$$K_P = \frac{q \cdot L}{A \cdot t(p_1 - p_2)} = \frac{(quantity\ of\ permeant)(thickness)}{(area)(time)(presure\ drop\ across\ the\ polymer)} \tag{A1}$$

The SI unit of permeability is [mol/(m s Pa)], although several other units are commonly used in scientific literature since the quantity of permeant can be expressed either in mass or in mole or in volume units. One of the most common units is called the *barrer [B]* and it is defined as follows:

$$1\ barrer\ [B] = 10^{-10} \left[\frac{cm^3(STP)\ cm}{cm^2\ s\ cmHg}\right] \tag{A2}$$

Where $cm^3$ (STP) is standard cubic centimeter, an amount unit expressed under condition of Standard Temperature and Pressure (STP) which correspond respectively to $T = 273{,}15$ [K] and $p = 10^5$ [Pa]. It is important to notice that $cm^3$ (STP) is not a unit of volume but a unit to express the number of molecules. Actually, it represents the molar quantity of gas that would take up 1 $cm^3$ at STP as calculated using the ideal gas law (A3)

See **Table A.1** for the conversion between the most frequently used units.

$$pV = nRT \tag{A3}$$

See **Table A.1** for the conversion between the most frequently used units [58].

**Table A.1:** Conversion factors between the most common units for gas permeability *[58]*

| into<br>from | $\frac{mol}{m\ s\ Pa}$ | $\frac{mol}{m\ d\ atm}$ | $barrer$ | $\frac{cm^3(STP)\ \mu m}{m^2\ d\ atm}$ | $\frac{cm^3(STP)\ mm}{m^2\ s\ atm}$ | $\frac{cm^3(STP)\ mil}{100in^2\ d\ atm}$ |
|---|---|---|---|---|---|---|
| $\frac{mol}{m\ s\ Pa}$ | 1 | $8{,}75 \cdot 10^{9}$ | $2{,}99 \cdot 10^{15}$ | $5{,}10 \cdot 10^{-21}$ | $4{,}40 \cdot 10^{-10}$ | $5{,}35 \cdot 10^{17}$ |
| $\frac{mol}{m\ d\ atm}$ | $1{,}14 \cdot 10^{-10}$ | 1 | $2{,}93 \cdot 10^{-6}$ | $4{,}46 \cdot 10^{-11}$ | 3,85 | $6{,}10 \cdot 10^{7}$ |
| $barrer$ | $3{,}34 \cdot 10^{-16}$ | $3{,}41 \cdot 10^{5}$ | 1 | $1{,}52 \cdot 10^{-5}$ | $1{,}32 \cdot 10^{6}$ | $1{,}67 \cdot 10^{2}$ |
| $\frac{cm^3(STP)\ \mu m}{m^2\ d\ atm}$ | $1{,}96 \cdot 10^{20}$ | $2{,}24 \cdot 10^{10}$ | $6{,}56 \cdot 10^{4}$ | 1 | $1{,}16 \cdot 10^{-8}$ | $6{,}45 \cdot 10^{-2}$ |
| $\frac{cm^3(STP)\ mm}{m^2\ s\ atm}$ | $2{,}27 \cdot 10^{9}$ | $2{,}59 \cdot 10^{-1}$ | $7{,}06 \cdot 10^{-7}$ | $8{,}64 \cdot 10^{7}$ | 1 | $5{,}59 \cdot 10^{6}$ |
| $\frac{cm^3(STP)\ mil}{100in^2\ d\ atm}$ | $1{,}87 \cdot 10^{-18}$ | $1{,}64 \cdot 10^{-8}$ | $6{,}00 \cdot 10^{-3}$ | $1{,}55 \cdot 10^{1}$ | $1{,}79 \cdot 10^{-7}$ | 1 |

## Appendix II: Owens-Wendt method for the estimation of surface energy

Owens and Wendt assumed that surface free energy $\gamma$ is defined by two components: London dispersion interactions $\gamma^d$ and polar $\gamma^p$ component [59]. The sum of $\gamma^d$ and $\gamma^p$ gives the total surface free energy $\gamma$, as reported in Equation (A.4).

$$\gamma = \gamma^d + \gamma^p \tag{A.4}$$

The estimation of solid surface free energy from contact angle is based on Young's equation (A.5), which correlates the angle of contact $\theta$ with the surface free energies of the liquid $\gamma_L$, and of the solid $\gamma_S$ and with the solid-liquid interfacial free energy $\gamma_{SL}$. (A.5)(A.5)

$$\gamma_L \cos\theta = \gamma_S - \gamma_{SL} \tag{A.5}$$

According to the assumption made by Owens and Wendt, Young's equation can be manipulated to give Equation (A.6).

$$\gamma_L(1+\cos\theta) = 2\sqrt{\gamma_S^d \gamma_L^d} + 2\sqrt{\gamma_S^p \gamma_L^p} \tag{A.6}$$

Where the subscripts $L$ and $S$ refer to liquid and solid respectively. Equation (A.6) allows determination of the surface free energy of a solid by measuring contact angle with two different liquids and by solving a system of two equations with two unknowns: $\gamma_S^d$ and $\gamma_S^p$.

In this work, distilled water and hexadecane have been used for the estimation of the surface free energy of the composite films. All the data on surface energies of these liquids are reported in **Table A.1**.

**Table A.1:** Surface energies, dispersion and polar components of water and hexadecane

| **Liquid** | **Total surface energy** **$\gamma$ [mN/m]** | **Dispersion component** **$\gamma^d$ [mN/m]** | **Polar component** **$\gamma^p$ [mN/m]** |
|---|---|---|---|
| Water | 72,8 | 21,8 | 51 |
| Hexadecane | 27,5 | 27,5 | 0 |

Since the polar component of the hexadecane is zero, simplified equations can be obtained for the calculation of the solid surface energy. Equations (A.7) and (A.8) give respectively the square roots of the dispersion and polar components of the surface energy of the solid sample under examination. The total surface energy can be obtained by the sum of these components.

$$\sqrt{\gamma_S^d} = \frac{(1+\cos\theta_h)\gamma_h}{2\sqrt{\gamma_h^d}} \tag{A.7}$$

$$\sqrt{\gamma_S^p} = \frac{(1+\cos\theta_w)\gamma_w - (1+\cos\theta_h)\gamma_h \cdot \sqrt{\frac{\gamma_w^d}{\gamma_h^d}}}{2\sqrt{\gamma_w^p}} \tag{A.8}$$

The subscripts $h$ and $w$ refer to hexadecane and water respectively.

# Ringraziamenti

Desidero ringraziare la prof.ssa Roberta Bongiovanni e la dott.ssa Sara Dalle Vacche per la loro disponibilità a fornirmi utili consigli e chiarimenti essenziali per la stesura di questa tesi.

Voglio ringraziare poi i miei genitori o, come sono soliti definirsi in maniera scherzosa, i miei “finanziatori” per avermi supportato durante tutto il mio percorso universitario, credendo sempre nelle mie capacità.

Ringrazio anche i miei raggi di sole, Federica e Agnese, che mi hanno sopportato durante le mie primissime sessioni d’esami, quando fischiettavo ossessivamente a qualsiasi ora del giorno e della notte. Se ho raggiunto questo obbiettivo è perché non mi hanno ucciso durante la triennale.

Devo ringraziare Fabio, il mio migliore amico, che più di tutti mi ha spronato in questi anni a dare sempre il massimo. Tra film orribili guardati insieme al cinema e serate passate a ballare e a bere, è sempre stato una costante per me ed è grazie a lui se a Torino ho vissuto esperienze indimenticabili che porterò per sempre con me.

Infine, voglio ringraziare Ludovica, la mia correttrice di bozze per le e-mail istituzionali. Durante questi mesi di scrittura della tesi siamo stati una valvola di sfogo l’uno per l’altra e alla fine ce l’abbiamo fatta entrambi.